BeFo

STIFTELSEN BERGTEKNISK FORSKNING
ROCK ENGINEERING RESEARCH FOUNDATION

SPECTRAL INFORMATION FROM FIELD SCALE TIME DOMAIN INDUCED POLARIZATION

Sara Johansson

BeFo Report 161

STIFTELSEN BERGTEKNISK FORSKNING
ROCK ENGINEERING RESEARCH FOUNDATION

SPECTRAL INFORMATION FROM FIELD SCALE TIME DOMAIN INDUCED POLARIZATION

Spektral information från tidsdomän inducerad polarisation i fältskala

Sara Johansson, Lund University

BeFo Report 161
Stockholm 2024
ISSN 1104 – 1773
ISRN BEFO-R—161—SE

This report is a representation of the Licentiate Thesis “From microstructure to subsurface characterization. Spectral information from field scale time domain induced polarization”.
Division of Engineering Geology, Lund University, 2016. I
ISBN 978-91-7623-673-4 (print), ISSN 978-91-7623-674-1 (pdf)
ISRN LUTVDG/(TVTG-1036)/1-99/(2016).
This BeFo report is published with the permission of the author.

Preface

Tomographic measurements of subsurface physical properties can be a valuable pre-investigation tool for many different kinds of infrastructure projects, including planning of tunnels, roads and buildings as well as remediation of contaminated soil. With the geophysical method spectral induced polarization (IP), several different geoelectrical parameters can be extracted through a single data set. The method has therefore a great potential of becoming an efficient and fast tool for characterizing several aspects of soils and bedrock. However, much remains to be known about how to analyse and interpret spectral IP parameters from field scale time domain IP measurements. Therefore, the main objective of this project is to focus on these issues.

This report is in parts based on a licentiate thesis; the work was supported by a reference group consisted of Gianluca Fiandaca, Per-Ivar Olsson, Lee Slater, Andy Binley, William Powrie, Robert Sturk, Thomas Günther, Roger Wisén, Andreas Pfaffhuber, Ulf Håkansson, Malin Ohlin, Staffan Hintze, Christel Karlsson, Thomas Sträng, Nils Otters and Per Tengborg.

The work was co-funded by Formas - The Swedish Research Council for Environment, Agricultural Sciences and Spatial Planning, SBUF - The Development Fund of the Swedish Construction Industry, Hakon Hansson foundation, Ernhold Lundström foundation and BeFo - Swedish Rock Engineering Research Foundation.

Stockholm

Patrik Vidstrand

Förord

Tomografiska mätningar av markens fysiska egenskaper kan vara ett värdefullt hjälpmedel vid förundersökningar för olika slags infrastrukturprojekt, t.ex. projektering av tunnlar, vägar och byggnader samt sanering av förorenad mark. Med den geofysiska metoden spektral inducerad polarisation (IP) kan flera olika geoelektriska parametrar extraheras ur ett enda dataset. Metoden har därför en stor potential att kunna bli ett effektivt och snabbt verktyg för att karaktärisera flera aspekter hos jordar och berggrund. Dock behövs forskning om hur spektrala IP parametrar från fältskaleundersökningar med tidsdomän IP bör analyseras och tolkas. Det huvudsakliga målet med detta projekt är därför att fokusera på dessa problem.

Rapporten är till delar baserad på en licentiatuppsats; referensgruppen för projektet bestod av Gianluca Fiandaca, Per-Ivar Olsson, Lee Slater, Andy Binley, William Powrie, Robert Sturk, Thomas Günther, Roger Wisén, Andreas Pfaffhuber, Ulf Håkansson, Malin Ohlin, Staffan Hintze, Christel Karlsson, Thomas Sträng, Nils Otters och Per Tengborg.

Projektet är samfinansierat av Formas - Forskningsrådet för miljö, areella näringar och samhällsbyggande, SBUF - Svenska Byggbranschens Utvecklingsfond, Hakon Hansson stiftelse och Ernhold Lundström stiftelse och BeFo.

Stockholm

Patrik Vidstrand

Summary

A large variety of subsurface infrastructure projects of different types can gain valuable information from tomographic measurements of subsurface physical properties. With resistivity and time domain spectral induced polarization (IP), the distributions of the conductive and capacitive properties of the subsurface are obtained. Technical developments of time domain IP equipment and new inversion algorithms have led to the possibility of collecting large amounts of data and invert for spectral IP parameters. In this way, much more information about the subsurface can be extracted from a single measurement compared to what was possible previously. It is well-known that spectral IP effects arise through redistribution of ions at the pore scale, and that spectral IP parameters can be linked to microscale surface chemical and structural properties. However, much remains to be known about how to analyze and interpret spectral IP parameters from field scale time domain IP measurements. Therefore, the main objective of this work is to focus on these issues.

In soils contaminated with free phase non-aqueous phase liquids (NAPLs), the contaminant phase affects the microgeometry inside the pore spaces of the soil. The results show that different configurations of the NAPL phase likely affect the spectral IP response of the soil in different ways. This is exemplified by measurements at a field site, where IP responses are absent in the NAPL source zone. In contrast, elevated IP responses are observed in the degradation zone, where the NAPL probably is configured as isolated droplets in the pore space. In order to investigate probable sources to observed varying IP responses in a Cretaceous limestone bedrock, the measured spectral IP parameters were compared with the investigations of the microstructure and composition of thin sections. Several characteristics that can affect the measurements were found, such as presence of certain minerals and varying texture of the limestone. However, more research is needed to understand the polarization mechanisms in limestones. Although most previous research has been carried out in sand- and claystones, there is a great potential to reveal textural and structural properties in any kind of bedrock by measurements of spectral IP parameters.

Keywords: Geophysics, Spectral Induced Polarization, Ground Investigation, Contaminant detection, Bedrock characterization

Sammanfattning

Många olika sorters underjordiska infrastrukturprojekt kan gagnas av den värdefulla information som tomografiska mätningar av markens fysiska egenskaper kan ge. Resistivitet och tidsdomän spektral inducerad polarisation (IP) ger en bild över markens distribution av konduktiva och kapacitiva egenskaper. Teknisk utveckling av mätutrustning för tidsdomän IP och nya inversionsalgoritmer har medfört möjligheter till att samla in stora datamängder och invertera för spektrala IP parametrar. På detta sätt kan mycket mer information om marken utvinnas från en och samma mätning, jämfört med vad som varit möjligt tidigare. Det är välkänt att spektrala IP effekter uppstår genom omfördelning av joner på porskalenivå, och att spektrala IP parametrar kan kopplas samman med ytkemiska och strukturella egenskaper på mikroskala. Dock behövs forskning om hur spektrala IP parametrar från fältskaleundersökningar med tidsdomän IP bör analyseras och tolkas. Det huvudsakliga målet med detta arbete är därför att fokusera på dessa problem.

I non-aqueous phase liquids (NAPL) förorenade jordar påverkar föroreningsfasen mikrogeometrin i jordens porsystem. Resultaten visar att olika konfigurationer av NAPL-fasen sannolikt påverkar den spektrala IP-responsen i jorden på olika sätt. Som exempel på detta förekom inga IP-responser i källzonen på en undersökt fältlokal. Dock observerades förhöjda IP-responser i nedbrytningszonen, där NAPL-fasen sannolikt är distribuerad som isolerade droppar i porsystemet. För att undersöka sannolika källor till de varierande IP-responser som observerades i en kalkstensberggrund kombinerades de uppmätta spektrala IP parametrarna med undersökningar av mikrostrukturen och sammansättningen i tunnslip. Flera egenskaper som kan påverka mätningarna identifierades, t.ex. förekomst av vissa mineraler och varierande textur i kalkstenen. Dock krävs mer forskning för att förstå hur polariseringsmekanismerna fungerar i kalkstenar. Trots att mycket forskning har fokuserat på sand- och lerstenar finns det en stor potential att mätningar av spektrala IP parametrar kan användas för att undersöka textur och strukturella egenskaper i alla sorts bergarter.

Nyckelord: Geofysik, Spektral Inducerad Polarisation, Markundersökningar, Föroreningsdetektering, Bergkarakterisering

Contents

Preface i
Förord iii
Summary v
Sammanfattning vii
Contents ix
1 Introduction 1
1.2 Objectives 2
2 Induced Polarization Measurements and Parameters 3
2.1 Time-domain Induced Polarization 3
2.2 Complex Resistivity 5
2.3 Electromagnetic interaction and normalized IP parameters 6
2.4 IP spectra and time decays 7
3 Phenomenological Models of IP spectra 9
3.1 The Debye and Cole-Cole models 9
3.2 Constant phase angle models 13
4 Physical Mechanisms of Induced Polarization 15
4.1 Electrode polarization 15
4.2 Membrane polarization 17
4.3 Electrochemical polarization 19
4.4 Interfacial (Maxwell-Wagner) polarization 21
5 Previous Research and Applications 23
5.1 Conductive minerals 23
5.2 Soils and sedimentary rocks 23
5.3 Pore water properties 24
5.4 Contaminated soil and microbiological processes 25
6 Methods & Materials 27
6.1 Time domain induced polarization measurements 27
6.2 Data processing 28
6.3 Data inversion 29
7 Main Results 33
7.1 Spectral IP responses of NAPL contaminated soil 33
7.2 Varying spectral IP responses in a Cretaceous limestone 36
8 Conclusions 39
8.1 Conclusions 39
9 References 41

1 Introduction

In many infrastructure projects, there is a need to obtain an image of the underground. Knowledge of rock properties are for example important during the planning of underground construction of tunnels, when questions about e.g. mechanical stability and risk of ground water flow arise. Other infrastructure projects deal with remediation of contaminated soils and search for methods to image extensions of contaminant plumes or the success of in situ remediation efforts. Drilling is a well-established method where detailed point information about the subsurface can be obtained, but there is a risk of missing important information in between the boreholes. Infrastructure projects often gain a better view of the investigated ground when drilling is combined with geophysical methods. Depending on the geophysical methods used, the variations in subsurface physical properties can often be linked to variations in geological or groundwater chemical properties. Whether the infrastructure project deals with geotechnical, environmental or other issues most fields working with soils, rocks and groundwater can benefit from knowledge that geophysical methods can provide.

Among physical properties of geological materials, electrical resistivity is the property that varies the most. The resistivity of earth materials varies from less than 1 Ωm (e.g. magnetite ores, certain clays) to more than 10^8 Ωm (e.g. marble and quartzite). The variations in resistivity are however large within each soil or rock type, which means that there is a large overlap in the resistivity range between different materials, and thus, it is not always possible to discriminate between them with resistivity alone.

To enhance the possibilities to discriminate between different materials or structures in the subsurface, the Induced Polarization (IP) effect can be measured simultaneously with the resistivity measurements. The IP effect is a measure of the ability of the soil to become polarized under the influence of an electric field, and the polarization properties of geological materials differ from the conductive properties measured with resistivity. During the polarization, energy is stored in the soil and one can make the analogy between electric potential energy (as stored kinetic energy) (Marshall & Madden 1959; Powers 1997). In time domain, the decay of the potential after the current interruption corresponds to the conversion of the stored energy back to electrical energy. It is known that the IP effect has a dispersive nature, meaning that the amount of polarization of the soil varies with the frequency (or time duration) of the injected current.

The existence of the IP effect has been known since the early 1900s, when it was discovered that sulfide mineralization gave rise to remnant potentials in the subsurface after the interruption of the transmitted current. Later, it was observed that many other geological materials also give rise to similar effects, however often weaker in magnitude. Although IP measurements early on were mostly used for mineral prospecting, they have more recently been applied for a wider range of investigations including landfill investigation (e.g. Dahlin et al. 2010), rock quality assessment (e.g. Magnusson et al. 2010) and estimations of hydraulic conductivity (e.g. Slater & Lesmes 2002).

The mechanisms behind the IP effect and its spectral behavior are not yet fully understood, which limits the interpretational possibilities of the method. A lot of research has been carried out in the laboratory in order to connect the IP signals to material properties. This research is mainly carried out in the frequency domain, and the samples are often carefully and homogeneously prepared. In this way, it has been possible to relate

the spectral IP response to a range of different petrophysical and chemical properties in the samples. The laboratory research has also served as a basis for some physical understanding about and modelling of different physical mechanisms behind the observed IP effect.

In the field, time domain measurements have a number of practical advantages over frequency domain measurements; they are more time efficient, robust and already common as pre-investigation methods in industry (Dahlin & Leroux 2012). However, in terms of interpretation of subsurface IP responses it is not straight forward to move from the relationships established with frequency domain laboratory measurements to time domain field results.

1.2 Objectives

The first objective of this work is to achieve an understanding of the physical mechanisms governing spectral induced polarization based on previous research. The second objective is to investigate how to analyze spectral induced polarization parameters from field scale time domain IP measurements. More specifically, the objective is to investigate if the distribution of contaminants in soils can be imaged with time domain spectral IP, exemplified by free phase dense non-aqueous phase liquids (DNAPLs). Furthermore, if spectral IP parameters can be used to obtain information of varying bedrock properties.

2 Induced Polarization Measurements and Parameters

The IP measurements performed in this work have been carried out in the time domain. However, a lot of previous knowledge about IP interpretation has been gained with frequency domain complex resistivity measurements (also referred to as spectral induced polarization measurements). Therefore, both techniques and the respective measured IP parameters are described in this chapter.

2.1 Time-domain Induced Polarization

Time-domain induced polarization (TDIP) is measured during the transmission of current pulses into the ground. A typical current waveform is shown in Figure 2.1., consisting of a cycle of square waves with alternating polarity and separated by current off times. Also shown in Figure 2.1. is the potential reading in one of the measurement channels. Apparently, it takes a certain time for the potential to reach its maximum value during the current transmission. Likewise, it also takes time for the potential to drop to zero after the interruption of the current transmission. This charge and discharge behavior of the ground is the basis for TDIP measurements.

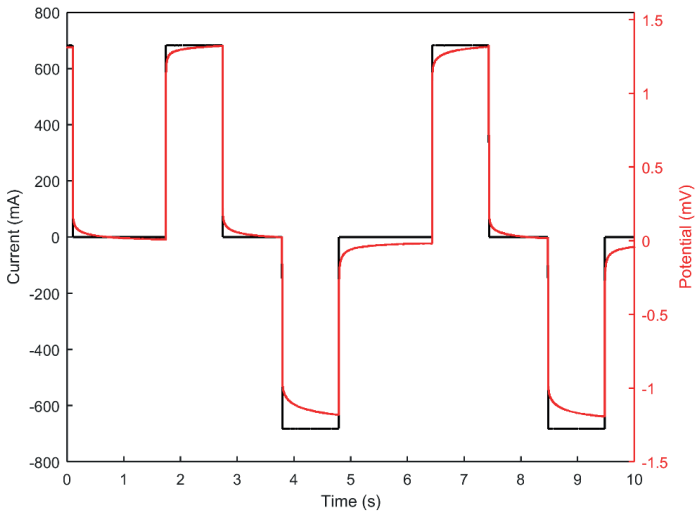

Figure 2.1. Typical current waveform (black) and potential response (red) in TDIP measurements.

While the resistivity is calculated from the maximum potential reading during the transmission of the current pulses, TDIP is a measure of how the potential declines after the current pulse has been interrupted. Figure 2.2 show a typical potential decay curve. Immediately after the current has been switched off, the potential drops to a so-called secondary response level, thereafter the shape of the potential decay curve is generally logarithmic (Sumner 1976).

The traditional measure of TDIP is a parameter called chargeability. The intrinsic chargeability was defined by Seigel (1959) as the magnitude of the secondary potential V_s to the primary potential V_p of the transmitted current wave:

Intrinsic chargeability $$m_0 = \frac{V_s}{V_p} \qquad (2.1)$$

Due to practical difficulties in measuring V_s immediately after the current interruption, the chargeability has traditionally been calculated through integration of the area beneath the decay curve during a defined time window:

Integral chargeability $$m_i = \frac{1}{t_2 - t_1} \int_{t_1}^{t_2} \frac{V_t}{V_p} dt \qquad (2.2)$$

where V_t is the potential reading at time t.

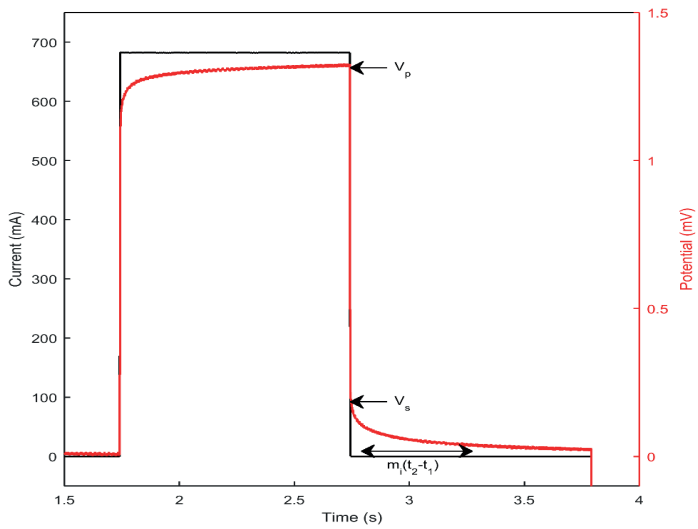

Figure 2.2. Illustration of the measures used to calculate the intrinsic or integral chargeability.

In practice, a discrete integration method is used with potential readings recorded in logarithmically spaced time gates (Sumner 1976). Both the gating and the duration of the

current pulses and off times have an important and inevitable effect on the magnitude of the integral chargeability. It is therefore often ambiguous to compare chargeability values between different materials in a similar manner as for example electrical resistivity. While resistivity is a material parameter, integral chargeability is highly dependent on measurement settings.

2.2 Complex Resistivity

Like DCIP, complex resistivity (CR) is a geophysical method used to measure the response of geological materials to transmitted electric. The main difference between the two methods is that the CR method works in the frequency domain. Instead of using square wave current pulses, a continuous alternating current is transmitted to the sample during CR measurements. The potential over the sample is measured and the phase- and amplitude shifts between the transmitted current and the received potential sinusoids are calculated (Figure 1.3). The alternating current frequency is swept through a range of frequencies, typically between at least 0.1-100Hz, resulting in spectra of amplitude- and phase values (Butler 2005; Sumner 1976).

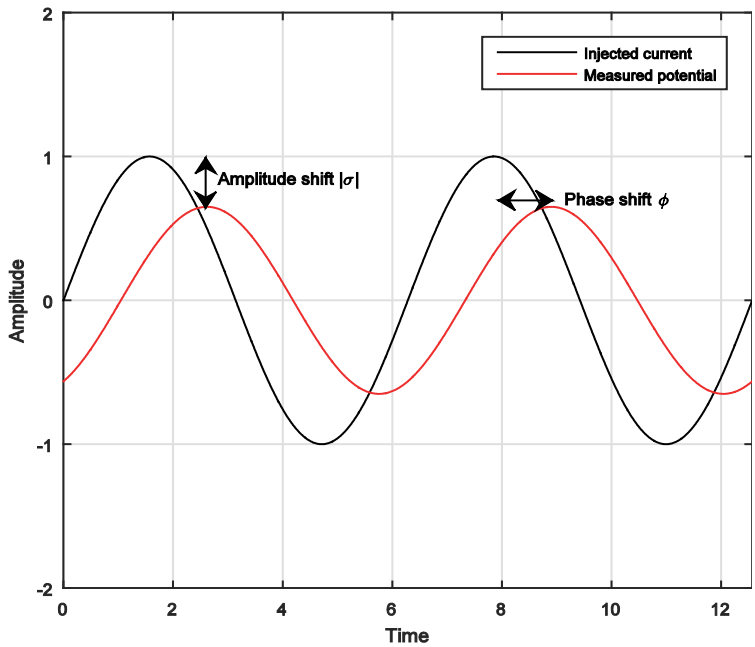

Figure 2.3. Illustration of the injected current and received potential in CR measurements and the extracted parameters.

In polar coordinates, the total complex resistivity ρ^* can be expressed as:

Complex resistivity $\rho^* = |\rho|e^{i\varphi}$ *(2.3)*

where $|\rho|$ is the magnitude of the amplitude and φ is the phase angle. In the literature, it is more common to express the measured complex quantity in terms of conductivity σ^* rather than resistivity ρ^*. From now on, this notation will therefore be used here also. For reasons that will become clear in the following chapters, it is often useful to express the complex conductivity in terms of the real (σ') and imaginary (σ'') components respectively:

Complex conductivity $\sigma^* = |\sigma|e^{i\varphi} = \sigma' + i\sigma''$ *(2.4)*

The real component is in-phase while the imaginary component is out-of-phase with the current waveform. The relationship between the measured parameters $|\sigma|$ and φ and the computable parameters σ' and σ'' is therefore of mathematical nature. The relationships can be written as:

Phase $\varphi = tan^{-1}(\frac{\sigma''}{\sigma'})$ *(2.5a)*

Amplitude $|\sigma| = \sqrt{(\sigma')^2 + (\sigma'')^2}$ *(2.5b)*

That is, the complex conductivity parameters φ and $|\sigma|$ are functions of both the real and imaginary components of the complex conductivity.

2.3 Electromagnetic interaction and normalized IP parameters

When a current is transmitted into the ground, an electromagnetic field is created which interacts with the media according to the electromagnetic theory. The relevant material properties for the interaction are the conductivity σ, the dielectric permittivity ε and the magnetic permeability μ. The magnetic permeability is mainly relevant when ferromagnetic minerals or materials are present in the soil (Butler 2005). Examples of ferromagnetic geological materials are pyrite (FeS_2) and magnetite (Fe_3O_4). Although most geologic materials are non-ferromagnetic and therefore do not have a significant magnetic permeability, all soils exhibit both conductive and dielectric behavior (Butler 2005).

The dielectric permittivity can be described as the ability of the material to become polarized in response to an electric field. Charges in the soil, which are not able to move freely, still react to an alternating electric field by displacing themselves in any way possible from their equilibrium positions. The charge displacements store energy from the electric field into the medium (Powers 1997; Butler 2005; Marshall & Madden 1959).

Since both the conductivity and the dielectric permittivity control motions of charges back and forth under the influence of a time varying electric field, it is not possible to only measure one of them from the total current density in the soil. The complex conductivity and the complex permittivity are two different measures of the same property. The measured complex conductivity will contain some influence of bound charges, while the measured complex permittivity will be affected by free charges. This means that whether

in time domain or in frequency domain, the measured resistivity and induced polarization are influenced by both conductive and dielectric properties of the soil.

In most geological media, the dielectric effects are small in comparison to the conductive and can therefore often be neglected during resistivity or conductivity measurements. The dielectric properties of the soil are, in contrast, often significantly influenced by the bulk conductivity of the soil. The bulk conductivity is a sum of the real valued ionic conductivity of the groundwater, the complex surface conductivity along interconnected particle surfaces and electronic conduction inside the grains.

Normalization of the chargeability or phase values with the measured conductivity yields the so called normalized IP parameters, which in many cases are useful approximations of pure polarization properties of the soil (Slater & Lesmes 2002b):

Normalized phase angle $\sigma'' = \varphi \cdot \sigma'$ *(2.6a)*

Normalized chargeability $MN = \frac{m_i}{\rho}$ *(2.6b)*

When the normalized IP parameters are used, it is assumed that the bulk conductivity is mainly made up of ionic conduction in the groundwater (i.e. that the contributions from surface conductivity and electronic conductivity are small) (Slater & Lesmes, 2002b). This assumption is valid for metal-free soils where electronic conduction in solid material is negligible. Most geologic materials are insulators, except e.g. metallic minerals such as pyrite and magnetite. Generally, the contribution of the electronic conduction to the electric conductivity of the soil becomes more important for low-porosity rocks, where the contribution from the ionic and surface conductions are small (Butler, 2005).

2.4 IP spectra and time decays

A physical basis for spectral IP is that different polarization processes in the soil take different amount of time to arise and decay. When the current is sent through the soil, charges start to move in accordance to the applied electric field. Therefore, it takes some time before the maximum potential is reached during the charging period. When the current is turned off (or the polarity is switched in frequency domain) the process is reversed, and the charges start to return to their original positions. The reversed process takes an equal amount of time to occur, which means that the charge and discharge (decay) curves are inverses of each other, at least theoretically. In other words, the polarization of the soil is theoretically a linear process, which means that Fourier transformation can be used to convert time domain IP data to frequency domain IP data and vice versa (Powers 1997; Sumner 1976). In time domain measurements, settings such as sampling rate and time duration of the current pulses affect how much spectral information is actually recorded (Kemna 2000; Van Voorhis et al. 1973). Time domain data corresponding to the fundamental frequency and harmonics of the square wave can be translated to phase spectra via Fourier transform. The method is described in detail in Van Voorhis et al. (1973).

There are however some practical difficulties related to the comparison of phase- and chargeability measurements. The magnitude of the measured phase values are limited by the frequency range used in the spectral induced polarization (SIP) measurements, while

the intrinsic chargeability in the time domain include the majority of the polarization response (Zonge et al. 1972). This could for example lead to an underestimation of the phase response if the main relaxation frequency is beyond the frequency range used in the measurements. In time domain, the underestimation of the intrinsic chargeability is most commonly caused by difficulties in gathering data from short times. It could also be caused by too short current pulses since the time would then be too short for the low frequency polarization mechanism to occur.

3 Phenomenological Models of IP spectra

Phenomenological models are equations that can be fitted to IP data in order to describe and parameterize the observed IP spectra or IP decays. These models are also used in inversion algorithms for extraction of spectral information from field data.

It has been argued that three main types of phase spectra have been observed in different SIP studies; spectra with a phase peak, nearly frequency independent phase spectra and spectra that increases with frequency (Titov et al. 2002). In addition, phase spectra with multiple phase peaks have also been reported (e.g. Nordsiek & Weller 2008). Several different kinds of models have been used to fit different kinds of IP spectra (see e.g. Dias 2000) and in this chapter, some of the most common phenomenological models in the literature are described.

3.1 The Debye and Cole-Cole models

The Debye equation describes the general behavior of the dielectric constant with a varying measurement frequency. The theory was developed for polar liquids, pictured as spheres in a viscous medium. The viscous medium represents molecular interactions that oppose the alignment of the dipoles according to the varying electric field. The frequency dependence of the dielectric constant is thus caused by the obstructed dipole polarization in this model. The complex dielectric constant ε^* in the Debye models is described as (Cole & Cole 1941):

Debye model $$\varepsilon^*(\omega) = \varepsilon_\infty + \frac{\varepsilon_0 - \varepsilon_\infty}{1 + i\omega\tau_0} \qquad (3.1)$$

where ε_∞ is the limiting (lower) value at high frequencies and $\varepsilon_0$is the limiting (higher) value at low frequencies. The measurement frequency is represented by ω, and τ_0 is a parameter called relaxation time. In the Debye theory, the relaxation time is proportional to the ratio between the macroscopic viscosity and the absolute temperature. This has the implication that the frequency range of the dispersion is low for solids (relatively high viscosity and large τ_0) and high for fluids. τ_0 is a measure of the time required for spherical dipoles to return to their original alignment after polarization. If the dipoles were assumed to be elliptical instead, three relaxation times would theoretically be obtained since the relaxation would occur along three axes (Cole & Cole 1941).

Cole & Cole (1941) observed that a broader frequency range of dispersion and adsorption could be seen in a wide range of experimental data, compared to what would be predicted from the Debye equation. As a result, they modified the Debye equation by adding the empirical exponent $(1 - \alpha)$ to equation 3.1, which gives the model an arbitrary flatter appearance (Cole & Cole 1941):

Cole-Cole model $$\varepsilon^*(\omega) = \varepsilon_\infty + \frac{\varepsilon_0 - \varepsilon_\infty}{1 + i\omega{\tau_0}^{1-\alpha}} \qquad (3.2)$$

The main difference between the Debye and the Cole-Cole model is that the Debye model represents the relaxation of a single particle size (in the above case a molecule). In contrast, the Cole-Cole model represents the relaxation of a range of sizes which broadens the spectra.

In the 1970s, Pelton et al. (1978) adopted the Cole-Cole model for complex resistivity data in frequency and time domain, introducing the intrinsic chargeability m_0 (equation 1.1) into the model (Pelton et al. 1978 and references therein):

Frequency domain Cole-Cole model

$$Z^*(\omega) = R_0\left[1 - m_0\left(1 - \frac{1}{1+(i\omega\tau)^c}\right)\right] \qquad (3.3)$$

where $Z^*(\omega)$ is the complex impedance (analogous to the complex dielectric constant) and R_0 is the DC resistivity. In this adoption of the Cole-Cole model, the exponent c (dimensionless, typically in the range between 0.1-0.6) is called the frequency dependence or the frequency factor. For a comparison between the Debye model and the Cole-Cole model with c =0.6, see Figure 3.1. The amplitude represents the real part of the complex impedance while the phase is the imaginary part. The time domain equivalent of the Cole-Cole model is given by (Pelton et al. 1978):

Time domain Cole-Cole model

$$V(t) = m_0 \frac{R_0}{I_0} \sum_{n=0}^{\infty} \frac{(-1)^n \left(\frac{t}{\tau}\right)^{nc}}{\Gamma(nc+1)} \qquad (3.4)$$

where $V(t)$ is the transient decay of the voltage after the disruption of the charging current I_0. In time domain, τ determines the length of time required for the main voltage decay. The effect of different relaxation times on the Cole-Cole model is plotted in Figure 3.2, in both time- and frequency domain.

In frequency domain, a single Cole-Cole model gives a symmetrical phase spectra where both sides of the peak have an equal slope (c and –c respectively). A variant of the Cole-Cole model, which gives an asymmetric phase peak, was presented in 1951 and is referred to as the Cole-Davidson model, see Figure 3.1. It can be seen that the slope of the Cole-Davidson model is similar to the Debye model on the left-hand side, while it approaches the slope of a Cole-Cole model (with c=0.6) at the right hand side. Both the Cole-Cole and the Cole-Davidson variants were combined in the so-called generalized Cole-Cole model 1983, where an additional exponent (a) was added to the denominator (Nordsiek & Weller, 2008 and references therein):

Generalized Cole-Cole model

$$Z^*(\omega) = R_0\left[1 - m_0\left(1 - \frac{1}{(1+(i\omega\tau)^c)^a}\right)\right] \qquad (3.5)$$

The Debye, Cole-Cole and Cole-Davidson models all presume a single phase peak in the IP spectra. However, multiple phase peaks have in some cases been observed in previous research. Depending on the shape of the spectra, Pelton et al. (1978) fitted their phase spectra with one or several Cole-Cole relaxations. An example of a double Cole-Cole model is plotted in Figure 3.1. An approach that allows even more flexibilities in possible shapes of the spectra is the Debye decomposition. Here, the observed IP spectra are decomposed into a number of Debye spectra. The observed real and imaginary parts of

the measured impedance $Z^*(\omega)$ are inverted in a process where values of chargeability are obtained from a predefined interval of relaxation times τ (Nordsiek & Weller 2008).

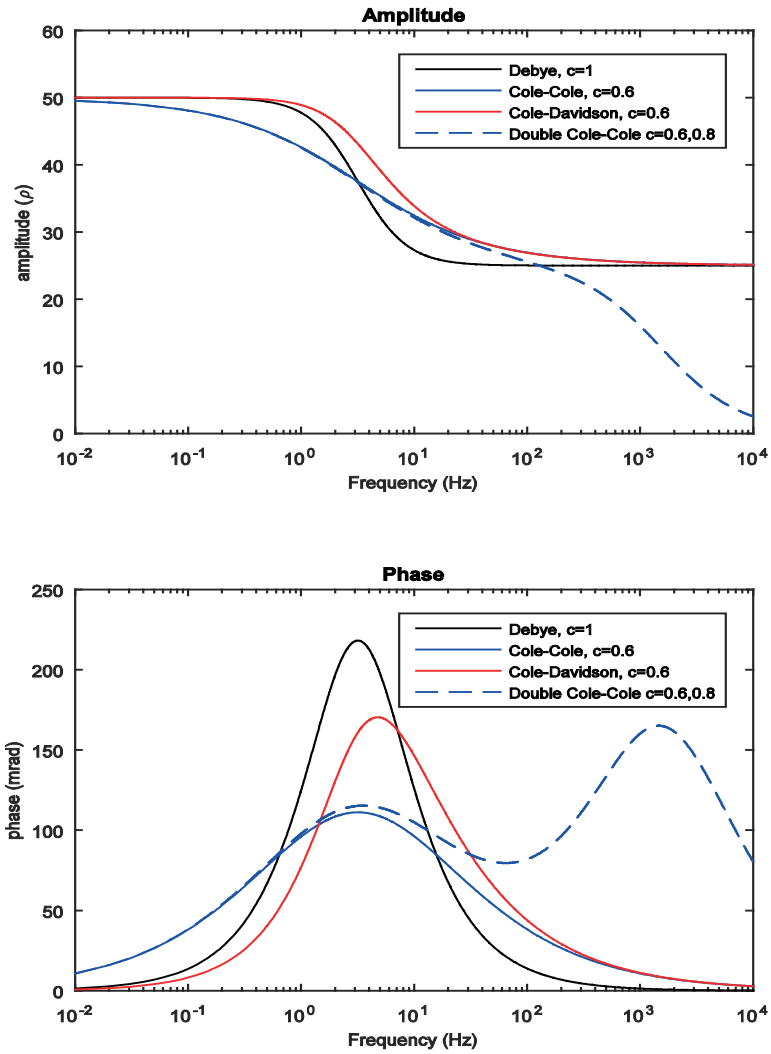

Figure 3.1. Comparison of common phenomenological models for IP spectra with phase peaks. $\boldsymbol{R_0}$*=50Ω,* $\boldsymbol{m}$*=500mV/V and* $\boldsymbol{\tau}$*=0.05s.*

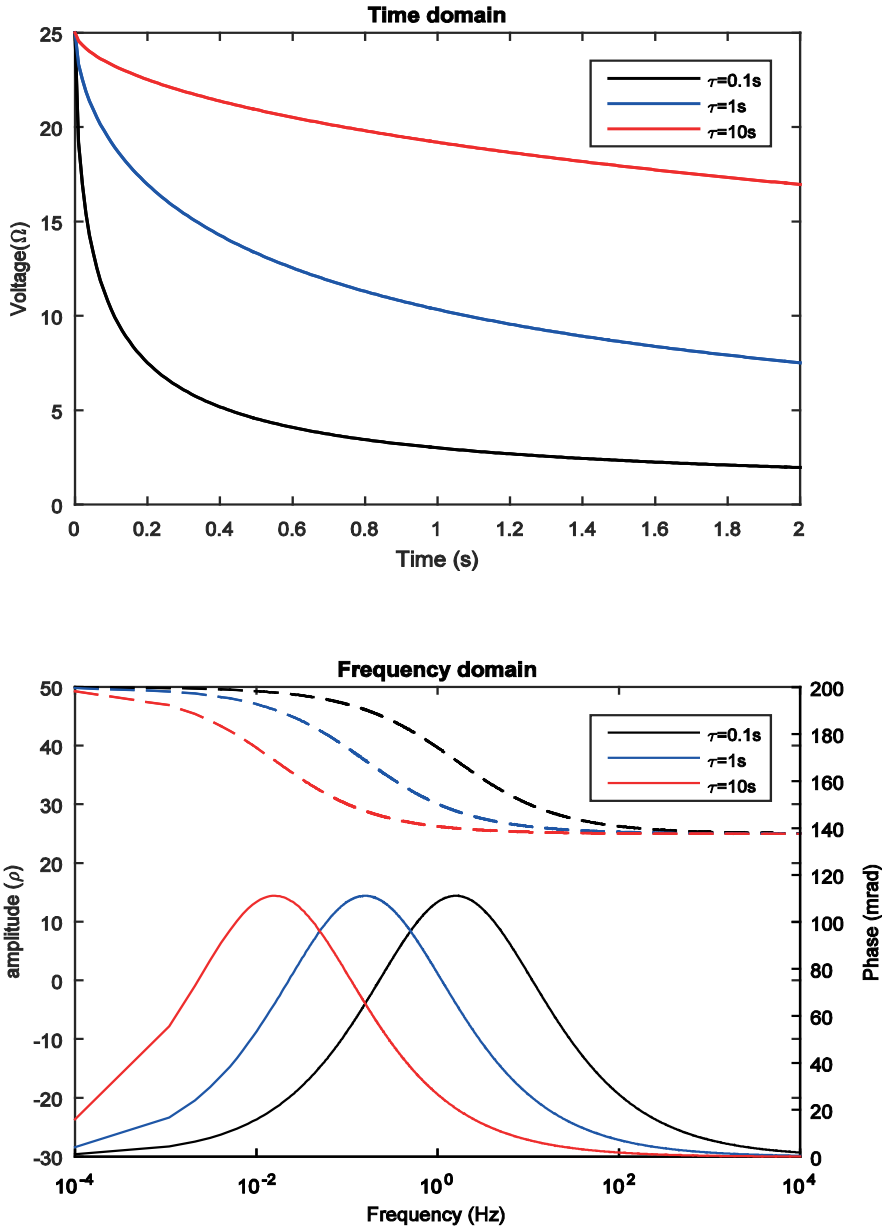

Figure 3.2. Variation of the Cole-Cole relaxation time in time domain (top) and frequency domain (bottom). In the bottom Figure, the dashed lines are the amplitudes and the solid lines are the phases. $\boldsymbol{R_0}$*=50Ω,* $\boldsymbol{m}$*=500mV/V and* $\boldsymbol{c}$*=0.6.*

3.2 Constant phase angle models

Constant phase angle (CPA) models are based on the idea that there is no frequency dependence of the measured phase angle. Based on their experiences from measurement on mineralized copper porphyry rock, Van Voorhis et al. (1973) constructed an empirical model to describe the shapes of their spectra (other variants of CPA models have also been described in the literature, see e.g. Lesmes & Friedman (2005)). Van Voorhis et al. (1973) observed a decrease of the amplitude with increasing frequency, while the phase was essentially constant. This behavior was described by their so-called Drake model:

Drake model $$\rho^*(\omega) = K(i\omega + \omega_l)^{-b} \qquad (3.6)$$

Where b is a positive fraction and K is an empirical constant. ω_l is a co-called low frequency pole, above which the phase spectrum is constant and the amplitude decreases. The positive fraction b determines the slope of the amplitude spectrum at frequencies above ω_l. The Drake model is plotted in Figure 3.3, where ω_l was set to 1Hz (for illustrative purposes. Generally, the low-frequency pole is set to much smaller values). At frequencies above ω_L, the phase is given by:

$$\varphi = -\frac{\pi}{2}b \qquad (3.7)$$

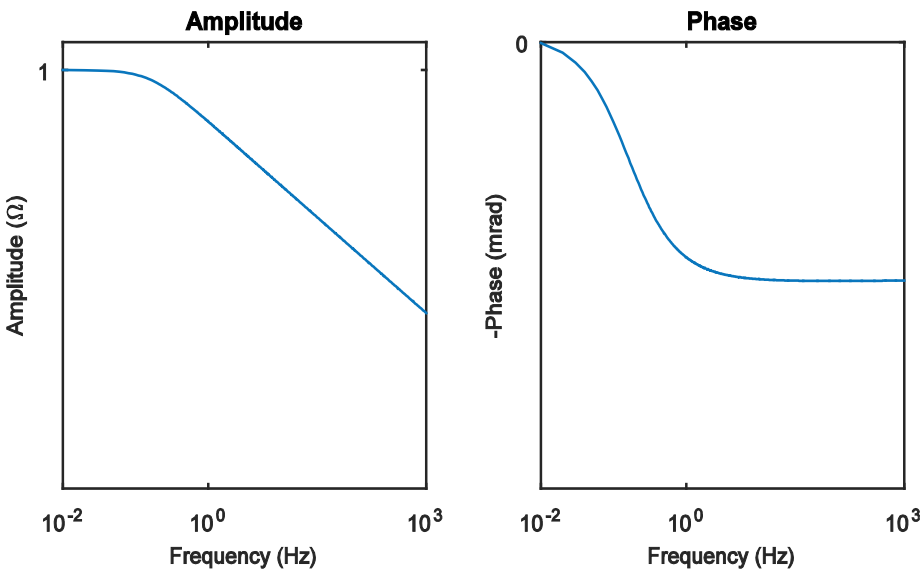

Figure 3.3. Illustration of the CPA model from Van Voorhis et al. (1973). $\boldsymbol{\omega_l}$*=1Hz.*

4 Physical Mechanisms of Induced Polarization

As mentioned earlier, the IP effect is a measure of the ability of the soil to become polarized when charges are displaced from their equilibrium positions. In a fundamental way, spectral IP is equivalent to electrochemical dielectric spectroscopy. In chemistry, dielectric spectroscopy is often used to analyze the properties of different fluids and other materials in a broad frequency range (up to the MHz range). Depending on the frequency, the charge displacement takes place through different mechanisms, e.g. electronic polarization which means that the circular orbits of electrons becomes elliptical, or orientational polarization when dipole molecules with a net neutral charge rotate into alignment with the electric field. As the frequency of the electric field (AC current) increases, the dielectric permittivity generally decreases since some of the polarization processes do not reach their fully displaced positions before the field reverses (Powers 1997).

SIP measurements are low-frequency dielectric spectroscopy measurements. At the relatively low current frequencies (usually below 1kHz), most polarization processes in the soil are related to redistribution of ions. Conceptually, the buildup and relaxation of different polarization mechanisms in the soil take different amounts of time to occur. With high current frequencies, there may not be enough time for the slowest mechanisms to completely arise before the electric field reverses its direction. This is one of the reasons why the amount of polarization varies with different current frequencies, and a spectral behavior of the IP effect is observed.

The difficulties in explaining the IP-effect in geological materials originate in the heterogeneity of soils and rocks at the microscale where the polarization processes occur. Varying mineral composition, microgeometry, chemical environment etc. makes it more difficult to understand how the polarization mechanisms work in the soils and rocks compared to more homogeneous materials. The measured IP-parameters are also often results of superimposed relaxations of several different polarization mechanisms occurring simultaneously in the soil. At present, there are four conceptual polarization mechanisms that can occur in the soil at the relevant frequencies, namely electrode polarization, membrane polarization, electrochemical polarization and interfacial (Maxwell-Wagner) polarization.

4.1 Electrode polarization

The electrode polarization mechanism is associated with conductive minerals in the soil (e.g. Sumner 1976; Ward 1988). When a conductive mineral is immersed into an electrolyte, its surface will become negatively charged. This will attract a fixed layer of positive counter ions in the electrolyte, called the Stern (or Helmholtz) layer (Figure 4.1). The ions in the fixed layer can be both electrostatically and/or chemically attracted. In addition, a second so-called diffuse layer is also formed by electrostatically attracted solvent ions. Both layers are collectively called the electrical double layer (EDL).

Two types of processes resulting in frequency dependent polarization can occur at the mineral-solution interface: faradic and non-faradic processes. The faradic processes are electrochemical redox reactions at the mineral-solution interface, i.e. electron transfer processes. Electron transfer between the minerals and the solution require that an energy barrier (reaction resistance) is crossed, which explains the impedance of the interface (Sumner 1976; Ward 1988). If the rate of redox reactions is high, the faradic processes are limited by the diffusion of ions to and from the mineral-electrolyte interface (Sumner 1976). When the rate of the redox reactions are limited, an excess of charge is found on the mineral surface (Bard & Faulkner 2001).

The faradic processes require the presence of active ion species in the electrolyte, which can take part in electrochemical redox reactions. Non-faradic processes involve non-active ions on the mineral surface. The non-faradic capacitance of the electrical double layer surrounding a mineral is directly comparable to a capacitor in an equivalent circuit. If no charge transfer occur, the two layers of charge can be compared to the two plates of a capacitor, separated by an insulating media (Wong 1979; Bard & Faulkner 2001).

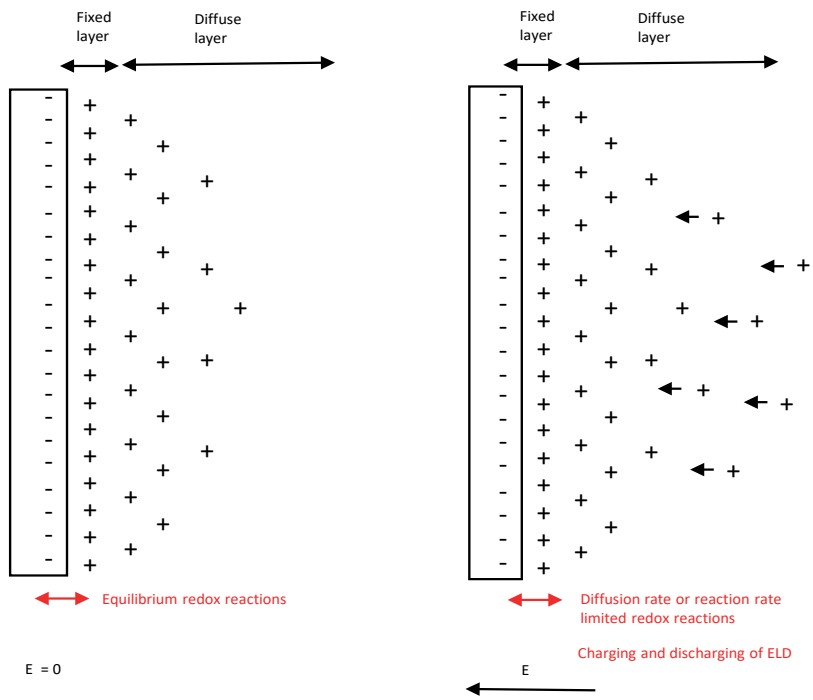

Figure 4.1. Conceptual sketch of the electrode polarization mechanism. The impedance of the metallic surface under the influence of an electric field arise due to unbalanced redox reactions and charging and discharging processes of the EDL.

The faradic processes and the EDLs around the minerals are in equilibrium when no electric field acts upon the soil (Sumner 1976). When an electric field is applied, ions in the electrolyte start to move and tend to accumulate at the surface of conductive minerals, since the different phases form a barrier for direct charge transport. The electrons in the mineral redistribute and balance the adsorbed excessive ions. With some faradic charge transfer between the mineral and the electrolyte, the system can be described as a "leaky" capacitor (Wong 1979). The capacitance is dependent on the rate of diffusion of active ions to and from the interface. While the impedance of a classical capacitor is inversely proportional to the current frequency ($1/(i\omega)$), the impedance of the metal-electrolyte interface is, because of the diffusion dependence, instead proportional to $1/\sqrt{i\omega}$ (and referred to as the Warburg impedance). At very low frequencies, the impedance is large and the soil acts as an insulator. At high frequencies on the other hand, the soil acts as a conductor and the impedance is low (Wong 1979; Sumner 1976; Marshall & Madden 1959).

The processes described above contribute to the impedance at the conductive mineral-electrolyte interface in two different ways. The non-faradic path represents the charging and discharging of the EDL under the influence of an alternating current. The faradic path represents the charge transfer across the interface, and the impedance is dependent on the redox reaction and ion diffusion rates. At low frequencies, most of the current is carried by the faradic processes while the non-faradic processes are dominant at higher frequencies (Ward 1988).

4.2 Membrane polarization

The membrane polarization model was first described by Marshall & Madden in 1959 in order to analyze and account for the so-called background polarization effects, which could not be explained by presence of conductive minerals. The concept of the membrane mechanism is the existence of a series of ion selective zones in the ground, regularly interrupted by zones with no ion selectivity. Ion selective zones are passages in the pore system where cations can pass while anions are blocked or vice versa. These zones can consist of narrow pores or pore-throats mainly occupied by cations in the EDLs of the surrounding grains (e.g. Titov et al. 2002), or of negatively charged clay particles attracting a cloud of positive counter ions (e.g. Marshall & Madden 1959; Ward 1988). A conceptual sketch of the membrane polarization mechanism is shown in Figure 4.2, where the alternating series consist of narrow ion selective pore throats and wider non-selective pores.

When an electric field is applied to the system, anions are blocked in front of the ion-selective zones while the cation diffusion is enhanced (membrane blocking effect), leading to an alternating series of ion surplus and deficiency along the pore space. With clay particles in the pore system, the cations attached to these will be displaced according to the electric field (Marshall & Madden 1959; Vinegar & Waxman 1984; Sumner 1976).

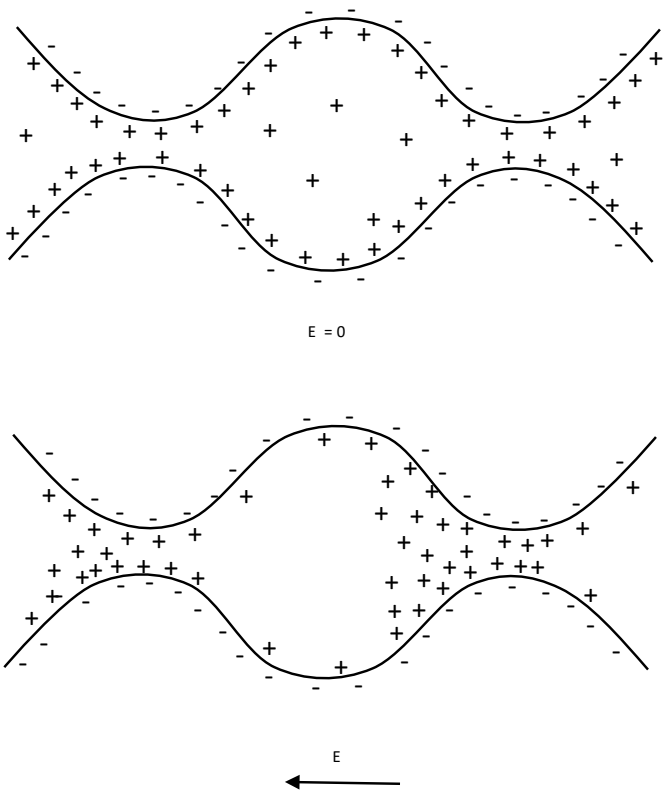

Figure 4.2. Conceptual sketch of the membrane polarization mechanism, where the ion selective zones consist of narrow pore throats. The mechanism leads to zones of ion surplus and ion deficiency around the narrow pores. Only cations are shown here for clarity.

The length ratio between ion selective and non-selective zones and the relative ion transparencies determines the amount of possible polarization. It is evident that if the ion selective zones occur too frequently, and essentially become continuous, no polarization will occur since no concentration gradient can develop without the non-selective zones. This situation can occur e.g. in very clay-rich shales (Sumner 1976; Marshall & Madden 1959; Vinegar & Waxman 1984; Titov et al. 2002).

The frequency dependence of the membrane polarization mechanism is diffusion controlled. The length of the ion selective and/or non-selective zones determines the length between the ion surplus and deficiency zones, and accordingly the relaxation times. According to Marshall & Madden (1959), the relaxation times are longer if the non-selective zones are longer than the selective zones. The relaxation time for a system similar to Figure 4.2 can be expressed as (Revil et al. 2012):

Membrane relaxation time $\tau = \frac{r^2}{2D}$ (4.1)

Where r is the characteristic pore size and D is the ion diffusion coefficient. According to (Titov et al. 2002), the peak relaxation time can be expressed as:

Membrane relaxation time $\tau = \frac{l^2}{4D}$ (4.2)

where l is the length of the selective zone. This is valid if the selective zone is much longer than the non-selective zone, an assumption referred to as the Short Narrow Pore (SNP) model (Titov et al. 2002; Titov et al. 2004). Regardless of whether it is the selective or non-selective zones that determines the relaxation time, the frequency dispersion increases with a large distribution of zone lengths (Marshall & Madden 1959; Vinegar & Waxman 1984).

4.3 Electrochemical polarization

Electrical double layers do not only form around conductive minerals immersed in an electrolyte; EDLs also form at the interfaces of electrically insulating minerals (e.g. silicates). When an electric field is applied to a geological media, the ions in the EDLs around the grains are redistributed. A conceptual sketch of the grain polarization principle is shown in Figure 4.3, where the EDL around a grain becomes polarized under the influence of the electric field. The grain polarization model clearly has some mechanisms in common with the membrane polarization model, i.e. the displacement of counter ions attached to particle surfaces.

The electrochemical polarization mechanism can be divided between polarization of the fixed and diffuse layers respectively since they react differently to an applied field. A theory for polarization of the fixed layer was developed by Schwarz (1962), who assumed that the ions could only move in a direction tangential to the grain surface. Surface conductivity along interconnected grains via their electrical double layers was not considered in this model.

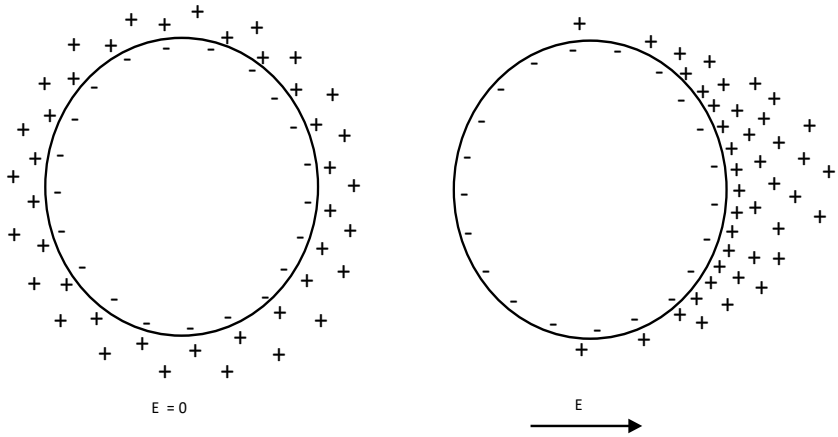

Figure 4.3. Conceptual sketch of the electrochemical polarization mechanism. Ions in the EDL are displaced under the influence of an electric field.

Later, both the fixed and diffuse layers were taken into account in models of the electrochemical polarization mechanism. The fixed layer polarization resulted in single Debye relaxation, while the diffuse layer showed a dispersion pattern more similar to a Cole-Cole relaxation. According to results of modelling, the fixed layer polarization is much stronger in magnitude than the diffuse layer polarization (de Lima & Sharma 1992; Lesmes & Morgan 2001). Polarization of the diffuse layer was later dismissed by Leroy et al. (2008) and Revil & Florsch (2010), who stated that the diffuse layer contributes to surface conductivity but not to polarization. The reason for the absent polarization is that the diffuse layers of the grains in a granular material are interconnected (Leroy et al. 2008; Revil & Florsch 2010).

In recent models, the mobility, ion densities and cation exchange capacities (CEC) in the fixed and diffuse layers are taken into account. The surface conduction is assumed to be dominated by the diffuse layer because of the low ion mobility in the Stern layer (Revil & Florsch 2010; Revil 2012).

The frequency dispersion of the electrochemical polarization mechanism is highly dependent on the grain size distribution. According to Revil & Florsch (2010), the peak relaxation time $\tau\ (s)$ of the peak soil polarization is related to dominant particle size d_0:

Electrochemical relaxation time $$\tau = \frac{d_0^2}{8D} \qquad (4.3)$$

where D is the diffusion coefficient of the ions. The frequency dispersion around the peak relaxation time is dependent on the grain size distribution, a wider distribution leads to a broader frequency dispersion.

4.4 Interfacial (Maxwell-Wagner) polarization

Maxwell-Wagner polarization is a mechanism that occurs at the interfaces between different materials in a composite material, and it is therefore also called interfacial polarization. A conceptual sketch of the mechanism in granular material is shown in Figure 4.4.

Different materials can be characterized by their electrical conductivity (σ) and dielectric permittivity (ε). The ratio between these properties (ε/σ) is the relaxation time (τ), and the relaxation time describes the required time for excess charges to spread in the material. In a simple case, charge builds up at a linear interface between two materials with different relaxation times:

Maxwell-Wagner relaxation time $$\tau_{MW} = \frac{\varepsilon_1 K_1 + \varepsilon_2 K_2}{\sigma_1 K_1 + \sigma_2 K_2} \qquad (4.4)$$

where ε_1, ε_2, σ_1 and σ_2 are the dielectric permittivities and electrical conductivities of the two materials. $K_1$and K_2 are geometrical factors which describe the ratio between the surface area of the interface and the thickness of the materials. The Maxwell-Wagner polarization process is therefore described by a single relaxation time τ_{MW}which is not equal to the relaxation times of the different materials (Iwamoto 2012). The accumulated charge at the interface is, at steady-state conditions:

Interfacial charge $$Q_s = (\tau_1 - \tau_2) \cdot J \cdot S \qquad (4.5)$$

Where τ_1 and τ_2 are the relaxation times of the materials, J (A/m^2) is the steady-state current density and S (m^2) is the interfacial surface area (Iwamoto 2012).

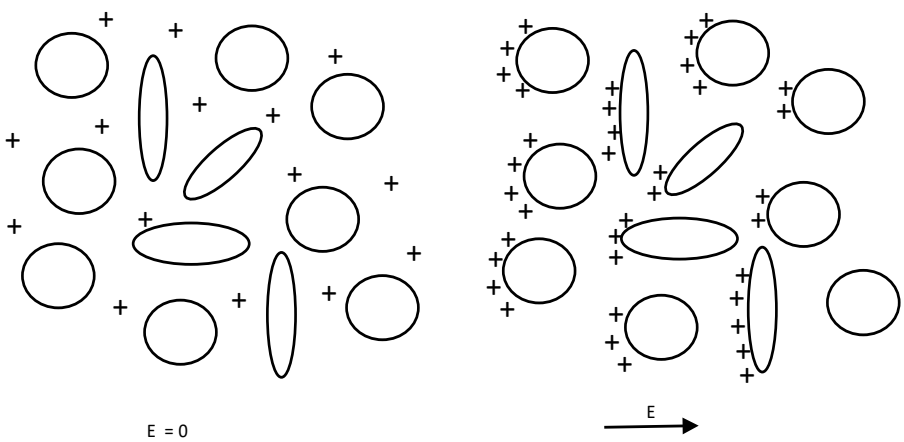

Figure 4.4. Conceptual sketch of the interfacial (Maxwell-Wagner) polarization mechanism.

Equations for more complex geometries than the simple case in equations 4.4 and 4.5 have been developed. The classical Maxwell-Wagner treatment describes the complex dielectric response of small concentrations of isolated spherical particles suspended in a medium. For larger concentrations, the Bruggeman-Hanai equation is considered more

appropriate. In both equations, the complex permittivity of the mixture is proportional to the complex permittivities and the relative volume fraction of the constituents (de Lima & Sharma 1992). The Bruggeman-Hanai equation was further developed by Sen et al. (1981) to incorporate Archie's cementation exponent m as a representation of particle shapes:

Complex permittivity $$\varepsilon^*(\omega) = \varepsilon_w^* \theta^m \left(\frac{1-\varepsilon_g^*/\varepsilon_w^*}{1-\varepsilon_g^*/\varepsilon}\right)^m \quad (4.6)$$

where ε_w^* and ε_g^* are the complex permittivities of the pore fluid and the grains, ε is the dielectric constant and θ is the volume fraction of pore fluid (Lesmes & Morgan 2001). At DC conditions, the Bruggeman-Hanai-Sen equation reduces to Archie's law (Sen et al. 1981; Lesmes & Morgan 2001):

Archie's law $$\sigma_{dc} = \sigma_w \theta^m \quad (4.7)$$

where σ_{dc} is the conductivity if the material and σ_w is the water conductivity.

Geometrical factors that affect Maxwell-Wagner polarization include for example existence of pore spaces isolated from the main conducting paths. The equations above assume that the pore space is interconnected, but existence of isolated pore spaces or pockets could give rise to higher dielectric permittivity at low frequencies (Sen et al. 1981). The Maxwell-Wagner polarization also appear to increase with small concentrations of grains with high aspect ratios in a host rock (Sen 1981).

The Maxwell-Wagner polarization mechanism arise due to intrinsic and geometrical properties of the geological material and is not dependent on surface electrochemistry. The two mechanisms are however superposed in geological media, and models that incorporate both interfacial and electrochemical polarization mechanisms have been developed (see de Lima & Sharma 1992; Lesmes & Morgan 2001; Leroy & Revil 2009).

5 Previous Research and Applications

The aim of this chapter is to give a brief description of previous research findings and applications for IP. The objective is to obtain an overview of areas where more research is needed, and the chapter does not give a complete review of the research field.

The research areas have here been divided into four sections: conductive minerals, soils and sedimentary rocks, pore water properties and contaminated soil and microbiological processes. The main motivation for IP measurements on conductive minerals has been ore exploration. Many studies on the IP responses of granular soils and sedimentary rocks and pore water properties have been carried out with the objective to image hydrogeological information, for example hydraulic conductivity (see e.g. Slater & Lesmes (2002) for a review). Another common motivation of IP research has been to develop methods for characterization of contaminated soil.

5.1 Conductive minerals

It has been known for a long time that certain minerals e.g. graphite, magnetite, pyrrhotite, pyrolusite and many sulfides produce high IP effects when they are disseminated in a host rock (e.g. Pelton et al. 1978). These minerals have in common that they are electrically conductive; other minerals containing similar elements do not give rise to strong IP effects due to their low electrical conductivity (e.g. Bertin & Loeb 1976).

In rocks or soils containing conductive minerals, the main polarization mechanism is electrode polarization. The IP magnitude is dependent on the concentration of conductive minerals. The spectral behavior in ores is dependent on the amount, size and geometry of the conductive minerals. When the mineralization occurs in veins and veinlets the observed relaxation times are generally very long. For discrete disseminated ores, the peak relaxation time is dependent on the grain size of the conductive minerals; large grain sizes leads to longer peak relaxation times, flatter spectra and decreased IP magnitudes compared to smaller grain sizes (Pelton et al. 1978; Wong 1979). Similar spectral IP behavior has been observed in sands containing conductive grains (Nordsiek & Weller 2008).

5.2 Soils and sedimentary rocks

Sands and sandstones have been studied a lot in previous research. Several relationships between IP spectra and petrophysical properties such as grain size distribution, specific surface area and pore throat size distribution have been found in the laboratory.

The amount of fine fractions (silt and clay) in a granular sample seems to play a significant role for the magnitude of the IP response; the IP magnitude generally increases with increasing amounts of fine fractions (Boadu & Owusu-Nimo 2010; Slater & Lesmes 2002a). Increasing clay content in sands and sandstones seem to play a particular role for observing high IP effects (Vinegar & Waxman 1984; Slater & Lesmes 2002a). The reason

is believed to be that clays generally have high specific surface area, which enables higher surface charge densities per unit volume.

The spectral dispersion in granular materials is generally considered to depend on the characteristic length scales over which the charges polarize (Slater & Lesmes 2002a). The relaxation time is in a homogeneous granular material dependent on either the grain size distribution (e.g. Revil & Florsch 2010; Titov et al. 2002; Leroy et al. 2008) or the distribution of pore throats sizes (e.g. Scott & Barker 2003; Binley et al. 2005). Similar to the case with conductive minerals, increased length scales (grain diameter or pore throat size) lead to longer relaxation times. It has also been observed that wider grain- or pore throat distributions leads to flatter polarization peaks (i.e. lower values of Cole-Cole frequency exponent c) (Scott & Barker 2003).

The specific surface area of grains in relation to pore volume (S_{por}) is one of the most important petrophysical parameters determining the magnitude of the IP effect (Slater & Lesmes 2002; Weller & Slater 2015). Binley et al. (2005) and Zisser et al. (2010) observed shorter relaxation times with increasing S_{por}. This was interpreted as an effect of the lower porosity in relation to the grain surface area leading to a greater number of small grains or pore throats being polarized. Similarly, Scott & Barker (2003) and Koch et al. (2011) observed that more densely packed grains seem to lead to shorter relaxation times, which could be an effect of smaller pore spaces compared to the conditions in more loosely packed grains.

Although increasing clay content in sands and sandstones tends to increase the IP response, research has shown that the IP responses of well-sorted clays usually are almost absent (Marshall & Madden 1959; Iliceto et al. 1982; Olhoeft 1985). Similarly, the studies by Iliceto et al. (1982) also indicated that the chargeability of well-sorted silt and loam was lower compared to the chargeability of natural sands. The absence of IP effects in clays were explained with the membrane polarization mechanism as a lack of zones with differing ion transparency (Marshall & Madden 1959). These conditions essentially lead to pure conduction along the grain surfaces without any ion displacements.

5.3 Pore water properties

Several studies have shown that the strength of the IP effect (chargeability or phase) decreases with increasing water content (e.g. Titov et al. 2004; Cassiani et al. 2009; Jougnot et al. 2010). In saturated samples, the main current path is via the electrolyte in the larger pores, meaning that the relative importance of the complex conductance through the EDL along the pore walls is relatively low. As the water saturation decreases and the larger pores drain, the relative importance of the complex conductance through the EDL becomes larger and the polarization increases (Titov et al. 2004). It can be presumed that the larger pore throats drain before the smaller ones, which has been reflected in the observation of shorter relaxation times with decreasing water saturation (Binley et al. 2005).

Normalized IP parameters seem to increase with groundwater salinity up to a certain point where after the magnitude starts to decrease with further increase in water conductivity (Vinegar & Waxman 1984; Lesmes & Frye 2001; Slater & Lesmes 2002a). The initial

increase can be attributed to increasing surface charge density, while the decrease at higher pore water salinity might be an effect of reduced surface charge mobility (Lesmes & Frye 2001) or an increased importance of the electrolytic (non-polarizable) conduction through the saline water (Scott & Barker 2003). While Scott & Barker (2003) observed a slight shift to shorter relaxation times, Vinegar & Waxman (1984) did not observe any strong frequency dependence with increasing water salinity.

5.4 Contaminated soil and microbiological processes

It is known that buried waste in landfills often produce large IP effects, and a number of studies have shown that chargeability or normalized chargeability mappings often are successful tools to delineate the waste body (e.g. Dahlin et al. 2010; Gazoty et al. 2012). Field IP measurements have also been performed with the aim to characterize soil contaminated with various kinds of substances, including BTEX and other hydrocarbons (e.g. Deceuster & Kaufmann 2012; Flores Orozco et al. 2012) or chlorinated solvents (e.g. Cardarelli & Di Filippo 2009). In the lab, several studies have dealt with the IP responses of contaminants such as e.g. oil or oil mixtures (Börner et al. 1993; Schmutz et al. 2010), waste- and motor oil (Vanhala 1997), gasoline (Martinho et al. 2006), octanol and benzene (Cassiani et al. 2009), toulene (Ustra et al. 2012), kerosene (Titov et al. 2004), ethanol (Personna et al. 2013) and trichloroethylene (Chambers et al. 2004). Many of the contaminants in the mentioned studies can be classified as non-aqueous phase liquids (NAPLs), which do not easily dissolve in water and often occupy the pore space as an own phase. There is no consensus on how NAPLs influence the measured IP response (Johansson et al. 2015) and more research is needed in this area (Kemna et al. 2012).

A complicating factor is that NAPL contaminated soils are subject to microbial degradation, which can lead to physical changes affecting the measurements. Microbial growth can lead to increased IP effects due to attachment of microbial cells around grains. It has been shown that EDLs forms around living cells which can affect the measured IP response (Atekwana & Slater 2009). Living or dead microbial cells can also change the pore geometry, for example by constriction of pores (Abdel Aal et al. 2006; Atekwana & Slater 2009). Furthermore, some bacterial activity involves precipitation of e.g. magnetite (Atekwana & Slater 2009) or calcite (Zhang et al. 2012). Microbial induced precipitation of sulfide minerals from the groundwater and corresponding measured increased IP effects have also been documented (Ntarlagiannis et al. 2005; Flores Orozco et al. 2011).

6 Methods & Materials

The overall methodology used in this work is to combine field scale DCIP measurements with micro-geometrical studies, since IP effects are known to arise at the microscale regardless of the measurement scale used.

The DCIP data that have been analyzed in Johansson et al. (2015) and Johansson et al. (2016) were collected during the same field campaign. The investigated site was selected since it is one of the worst PCE contaminated sites in Sweden, and the main objective was to investigate if the PCE contamination could be delineated with DCIP. Another objective was to characterize the soil- and bedrock conditions in the surrounding area to aid the risk assessment for polluted groundwater dispersal.

6.1 Time domain induced polarization measurements

The ABEM Terrameter LS was used to collect resistivity and time domain IP data along 2D sections with the cable and electrode layout shown in Figure 6.1. Separated cables for injecting current and measuring potential were used in order to reduce capacitive coupling effects (Dahlin & Leroux 2012). The extra cables were connected to the instrument via an external relay switch (ES10-64).

To further reduce capacitive coupling and to increase the signal-to-noise ratio, low contact resistances between the electrodes and the ground were secured by a Focus One electrode contact test (Dahlin & Leroux 2012). When needed, the contact resistance was reduced by adding a starch-water mixture around the electrodes.

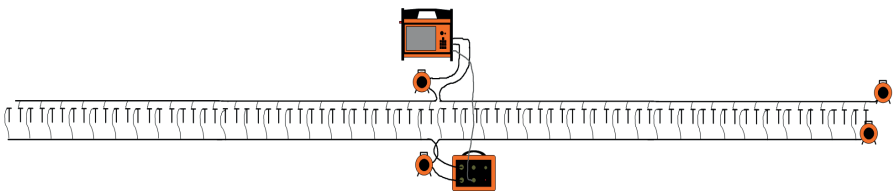

Figure 6.1. Separated cable layout used for the DCIP measurements.

The pole-dipole electrode configuration was used in order to acquire data of both high spatial resolution and large depth penetration (Dahlin & Zhou 2004). The spacing between the electrodes was 2.5m, except in one case when a road was crossed and electrodes were excluded from the measurement protocol. Cables with 5m spacing between the 21 electrode take-outs were used. For the shorter measurement profiles (Johansson et al. 2015), 42 electrodes or less (due to lack of space) were in use in the electrode spread. This corresponds to a maximum profile length of 102.5m and depth penetration of around 27.5m. In the longer measurement profiles (Johansson et al. (2016)), all 84 electrodes were in use which resulted in 207.5m long measurement profiles with a maximum depth penetration of approximately 75m. The on- and off-times of the

current pulses were 1s long, and full waveform data was collected with a sampling rate of 1000Hz.

6.2 Data processing

Since the data was measured in an urban area, it was affected by noise. The main sources of periodic noise were power line and train traffic noise at frequencies of 50Hz and 16 2/3Hz. The periodic noise was reduced by using multiples of 60ms (equivalent to one period of 16 2/3 Hz and three periods of 50Hz) in the gating of the IP data. The delay time was 1ms and the gates were logarithmically spaced in between 0.07-0.97s.

Before inversions in AarhusInv, all decays were processed in Workbench. In Workbench it is possible to remove single IP gates and keep the remaining part of the decays. Typical bad IP gates are gates at early times, which may be affected by inductive coupling, or late times, which may be affected by electrode polarization effects. Examples of unprocessed decay curves are shown in Figure 6.2.

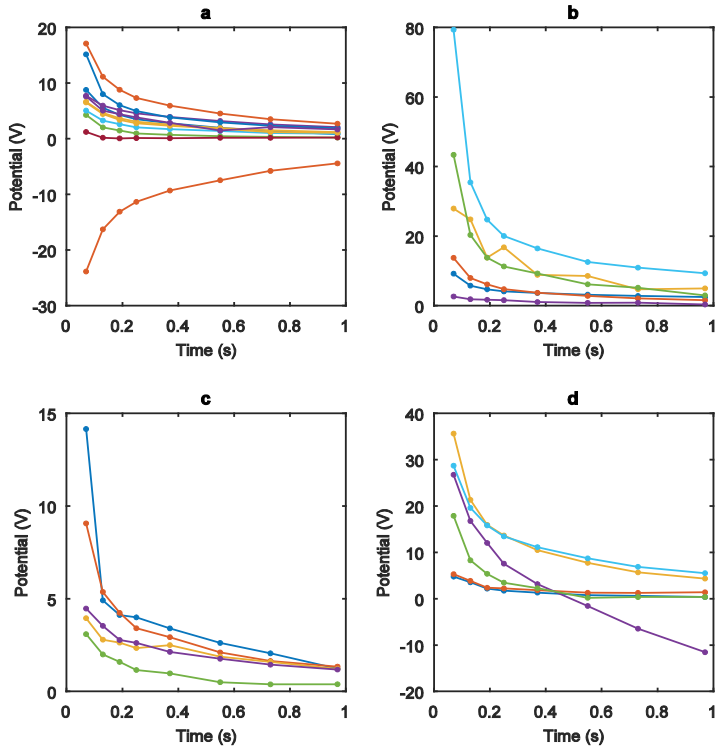

Figure 6.2. Examples of unprocessed decay curves. (a) a negative decay curve. (b) noise affected decay curve (yellow) (c) a decay curve with a disturbed first time gate (blue) (d) Disturbed decay curve becoming negative after ~0.5s (purple).

A noise affected decay curve can be seen in Figure 6.2b, and a decay with too high values in the first gate is shown in Figure 6.2c. In Figure 6.2d, one of the decay curves becomes strongly negative at later times. In some cases, single gates in the middle of the decays were removed if the quality of the decay looked good for the rest. Negative IP decays (fig 6.2a) were generally not regarded as bad data quality, since they may be caused by geometrical distribution of chargeable bodies in zones of negative sensitivity (Dahlin & Loke 2015). In some cases, there might also be physical mechanisms behind negative IP decays (Brandes & Acworth 2003).

6.3 Data inversion

The inversions of processed data were made in AarhusInv (Fiandaca et al. 2012; Fiandaca et al. 2013). In the forward response modelling, the complex conductivity distribution is calculated in a finite element mesh for a number of frequency decades. The model space is then defined by frequency, resistivity and the spectral IP parameters of the Cole-Cole or the CPA model. The complex impedance transfer function of the system can be calculated for any electrode quadruple and be transformed to a potential response in time domain via inverse Fourier transform. The finite length of current pulses in time domain measurements and the stacking procedure can affect the potential response considerably. The transmitted waveform and received potential response is therefore modelled and superposed in the forward response (Fiandaca et al. 2012; Fiandaca et al. 2013). The data and the forward response are then used in an iterative inversion process, where the misfit between the data and the model is minimized (Auken et al. 2014).

In Johansson et al. (2015), the data was inverted with both the Cole-Cole and the CPA models, although the Cole-Cole inversion of the data was considered uncertain due to the short measured time interval (0.07-0.97s). The data were inverted using L2-norm constraints with horizontal and vertical constraints of 7.5% and 25% respectively. The model fit was checked via a visual comparison between the measured and the inverted decays. An example of a good model fit with the CPA model is shown in Figure 6.3a. For the decays in Figure 6.3b, the CPA model underestimates the potential values at early times. In this case, a Cole-Cole model may fit the data better.

For Johansson et al. (2016), a new signal processing scheme was available which enabled recovering of early decay times (Olsson et al. 2016). The time interval 0.009-0.974s was used, and the extra decade of data increased the possibilities of recovering spectral information during the inversions for Johansson et al. (2016). In addition, shorter relaxation times were generally expected in the consolidated limestone analyzed in Johansson et al. (2016), compared to the unconsolidated soils which were in focus in Johansson et al. (2015). For these reasons, the Cole-Cole model was used for the inversions in Johansson et al. (2016). The data were inverted using L2-norm constraints with horizontal and vertical constraints of 15% and 50% respectively.

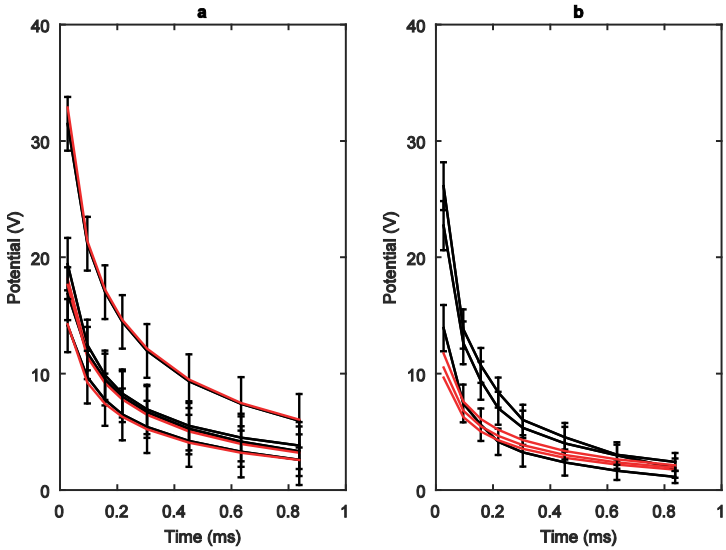

Figure 6.3. Fit between data (black) and CPA inverted decays (red). The model underestimates the chargeability in (b), where the decays likely contain spectral information.

6.4 Interpretation

The inverted data that were analyzed in Johansson et al. (2015) were measured on a site contaminated with tetrachloroethylene (PCE). PCE is a dense non-aqueous phase liquid (DNAPL), and the physical properties of the contaminant infer that it affects the pore geometry of the investigated soil.

The inverted results were initially compared with borehole data of DNAPL concentrations collected at the site, but the direct comparison did not show any strong correlation with the resistivity or IP anomalies. Previous experiences from similar investigations were therefore sought in the literature. However, no consensus was found in the results of previous research, and several different conceptual models of NAPL geometry in the pore space have been used to interpret data from both laboratory and field studies. Therefore, the probable effect of possible NAPL configurations on the spectral IP response of a granular material (based on current knowledge of physical mechanisms, see chapter 4) was discussed in Johansson et al. (2015). Both interpretations from previous research and novel ideas were considered.

The possible NAPL configurations were based on the common physical properties of the fluids and on previous research in the fields of petrophysics and environmental research. Since the geological material at the investigated site consists mainly of sandy chalk till (in which no large IP effects are expected), the simple conceptual models discussed in Johansson et al. (2015) were considered accurate enough to guide the interpretation of the IP responses measured at the site. In a more complex geological setting, the conceptual models in Johansson et al. (2015) might not be applicable.

The inverted data in Johansson et al. (2016) were also ambiguous to interpret. Varying resistivity and spectral IP responses were found in the investigated limestone bedrock.

Since IP investigations of limestones are not common in the literature, the microstructure and composition of limestone from the Kristianstad basin were investigated. General characteristics and a detailed lithological analysis of a nearby deeply drilled core were available in the geological literature. Access to drill cutting samples was also provided by an entrepreneur working in the Kristianstad basin after the DCIP survey. These samples were investigated with Scanning Electron Microscopy (SEM) and Energy Dispersive X-ray Spectroscopy (EDS) and provided detailed information of varying microstructure and mineral composition at different levels of the limestone. The geological characterization of the investigated limestone served as a basis for the interpretation of the varying IP responses measured at the site.

The field data interpretations presented in the next chapter are rather theoretical and qualitative than empirical and quantitative. Quantitative results of field data can be uncertain for several reasons, including insufficient amount of reference data for statistical significance and different measurement accuracy of the compared quantities. For example, the spatial accuracy of the borehole contaminant concentrations used in Johansson et al. (2015) are high, while the corresponding IP responses are representative of a relatively large soil volume. Data quality, processing and inversion also infer uncertainties in the exact accuracy of the inverted IP values. Qualitative interpretations of field data that can be theoretically supported by micro-geometrical properties might also have a larger potential for providing results which can be useful and applicable in future field studies.

7 Main Results

7.1 Spectral IP responses of NAPL contaminated soil

Previous results from field and laboratory IP investigations on NAPL contaminated soil vary a lot and point in opposite directions. In Johansson et al. (2015) previous research is reviewed and DCIP field results are presented, measured at a tetrachloroethylene (PCE) contaminated site.

The four possible configurations of NAPLs in a water saturated pore space that were discussed in Johansson et al. (2015) are shown in Figure 7.1. Depending on factors such as e.g. concentration, oil wettability and vertical or horizontal location in the contaminant plume, the NAPLs can be present in pores or pore throats of the granular material, interconnected through several pores or coating grain surfaces (Figure 7.1a-d).

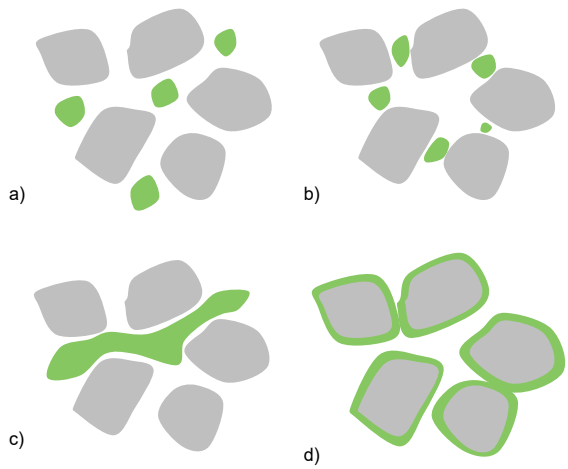

Figure 7.1. Different conceptual models of possible NAPL configurations in a granular pore space (modified from Johansson et al. 2015). The different models are expected to affect spectral IP parameters in different ways, see Table 7.1.

Expected spectral IP (Cole-Cole) responses of these systems (Table 7.1), theoretically based on the electrochemical and membrane polarization mechanisms, were discussed and presented in Johansson et al. (2015).

Table 7.1. Expected spectral Cole-Cole responses of the NAPL configurations in Figure 7.1 (modified from Johansson et al. 2015). The responses are discussed in Johansson et al. (2015) and are based on the electrochemical (EC) and membrane (M) polarization mechanisms.

Conceptual model	Chargeabiliy (m_0)		Relaxation time (τ)		Frequency factor (c)	
	EC	M	EC	M	EC	M
A	increase	increase	decrease	decrease	decrease	decrease
B	increase	increase	decrease	unchanged	decrease	unchanged
C	decrease	not present	unchanged	not present	decrease	not present
D	increase or decrease	increase	increase	decrease	decrease	decrease

The field results in Johansson et al. (2015) showed that enhanced IP effects appeared next to the PCE source zone, i.e. not at the location where the highest concentrations of free phase contaminants had been measured (Figure 7.2). At the locations of the phase anomalies, the measured PCE concentrations were intermediately large. The enhanced phase and normalized phase were therefore interpreted as a representation of a degradation zone, where partial degradation of the free phase PCE has resulted in a NAPL configuration similar Figure 7.1a. According to the electrochemical and membrane polarization mechanisms, such a NAPL configuration is expected to give rise to an enhanced IP response compared to the IP response of a clean soil.

In contrast to this, a NAPL configuration similar to Figure 7.1c is expected to decrease the IP response of a contaminated soil. This could explain why no phase anomalies are present in the source zone where the highest PCE concentrations have been measured, since high concentrations increase the probability of interconnected NAPL in the pore space. More research is needed to validate the influence of different NAPL configurations on the spectral IP response, but it is likely that these results at least partly can explain why varying results have been achieved in previous research.

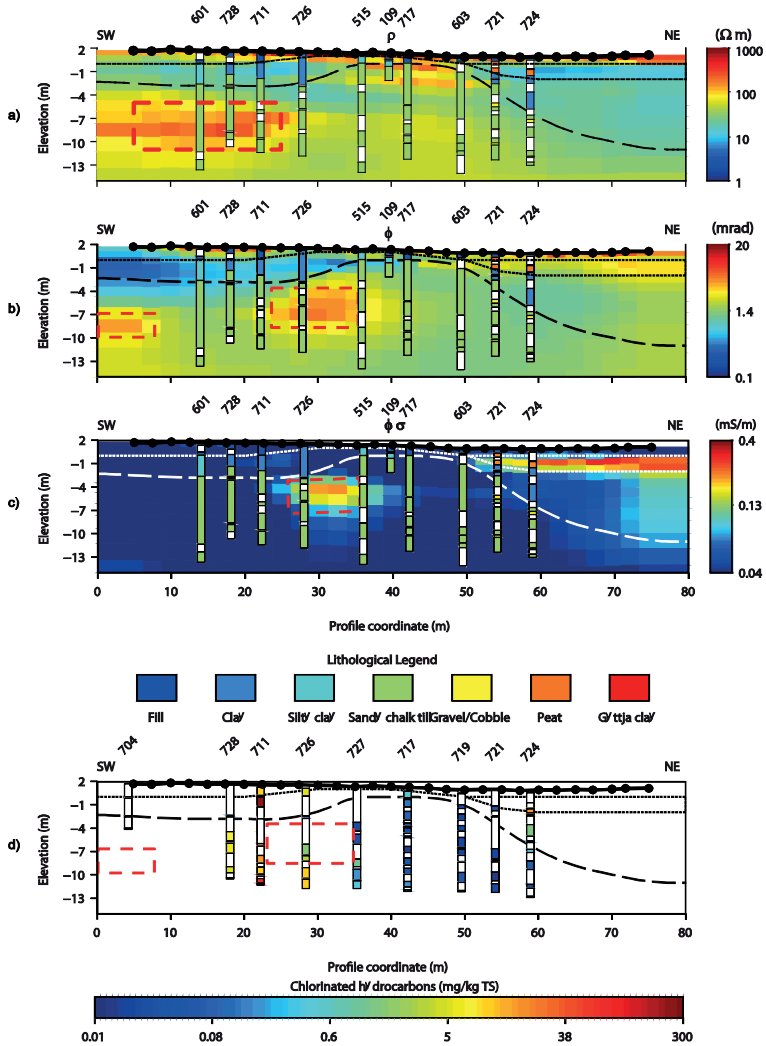

Figure 7.2. Field results from the investigated site, showing sections of resistivity (a), phase (c) and normalized phase (c) with superposed geological borehole information. Total chlorinated hydrocarbon concentrations measured in the boreholes are shown in d. Increased phase and normalized phase values can be observed at the border of the PCE source zone (as indicated by high chemical concentrations in (d) (Johansson et al. 2015)).

7.2 Varying spectral IP responses in a Cretaceous limestone

In previous research, resistivity and IP has been used to map fractured and weathered zones in bedrocks. In studies of silicate-based rock types, zones with low resistivity and high chargeability have been indicators of clay weathered fracture zones, where the clay is responsible for the elevated IP responses. In the Cretaceous limestone (Kristianstad basin) investigated in Johansson et al. (2016), weak IP responses were expected. However, anomalous zones of elevated normalized chargeability and low resistivity were found. The low resistive zones could indicate e.g. fracture or karst zones, but clay weathering processes are naturally limited in limestones. In a weathered limestone, the dissolution of calcium carbonate would rather be expected to lead to decreased IP responses. It was therefore uncertain how to interpret the detected zones of elevated normalized chargeability in Johansson et al. (2016).

Since the main survey area in Johansson et al. (2016) was located in an urban environment where it could not be completely excluded that noise and 3D-effects distort the DCIP results, a reference line was also measured in a rural area approximately 4km from the main survey site. The Cole-Cole inverted results from the reference line are shown in Figure 7.3. At this location, the limestone bedrock surface is located a few meters below the ground surface. Figure 7.3a-d shows that the resistivity and the Cole-Cole parameters varies in the bedrock. Previous research has shown that normalized chargeability (Figure 7.3e) often describes structural surface polarization properties better than chargeability (Figure 7.3b). Although the normalized chargeability generally is low in the limestone, anomalous zones of elevated values can be observed. Interesting variations in Cole-Cole relaxation time and frequency factor (Figure 7.3b-c) could possibly reflect textural variations within the limestone. Since no man-made constructions or installations are present in vicinity of the reference line, these results confirm that variations in IP response can be linked to the limestone composition or structure.

The analysis of the drill cutting samples from a borehole in the Kristianstad basin showed that the character of the limestone varied between different levels, from almost pure calcium carbonate-based limestone to limestone with quartz and feldspar grains and clay matrix. Varying presence of clay matrix could be a possible explanation to varying IP responses of the limestone. In addition, pyrite minerals were detected in most of the core levels, as well as glauconitic sand (Figure 7.4). Varying presence of these minerals could also be an explanation of varying IP responses within the limestone.

A lithological analysis of a relatively closely located core in the Kristianstad basin confirms variations in micro-geometrical properties in the limestone. The variations in this core originate from a varying sedimentation environment during the formation of the limestone. Local depressions or channels in the bedrock at some point or collapsed karst cavities could explain vertical variations in the microgeometry.

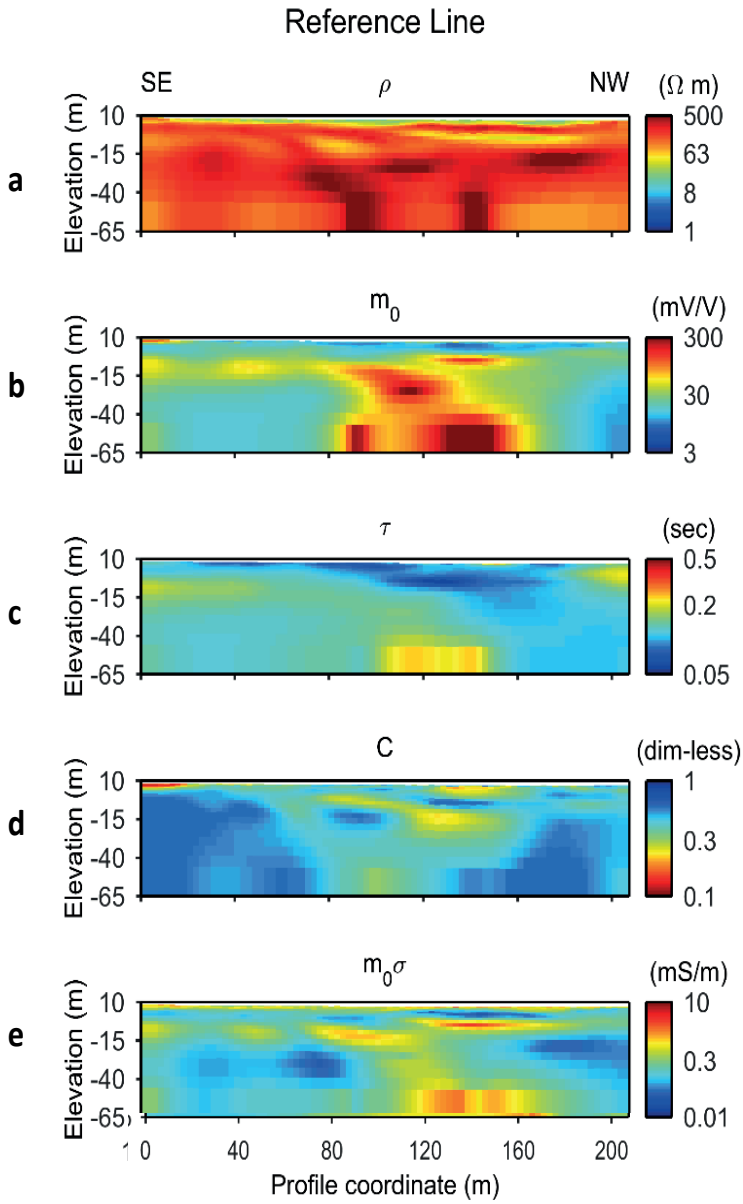

Figure 7.3. Variations in Cole-Cole parameters and normalized chargeabiltiy measured in a Cretaceous limestone bedrock (Johansson et al. 2016)

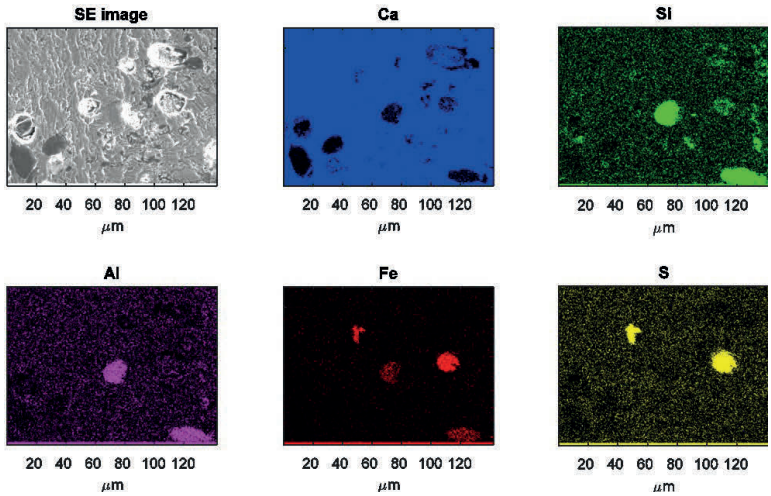

Figure 7.4. SEM and EDS results from a limestone sample, showing prescence of both pyrite (indicated by Fe and S) and glauconitic grains (indicated by Si, Al and Fe) within the limestone (modified from Johansson et al. 2016). The amounts of pyrite and glauconite varied at different levels in the core.

8 Conclusions

8.1 Conclusions

Interpretation of field data is not always straight forward – many unknown factors could influence the IP response of the subsurface. It is crucial to initially evaluate if observed IP effects could be a result of bad data quality, 3D-effects or noise, especially when the data have been measured in urban environments. Secondly, it is important to obtain an acceptable fit between the data and the inverted model. With spectral inversion, this involves an assessment of which phenomenological model (e.g. the Cole-Cole or the CPA model) the data should be fitted with.

From this work, it can be concluded that it is possible to obtain spectral IP models of consistent quality from time domain IP measurements in an urban environment. This is a result of new developments in data acquisition techniques, data processing and inversion methods. Challenging conditions with periodic noise from train traffic and power lines is handled with improved data filtering. Although it is more favorable to measure with longer time pulses, it has been shown that under certain conditions, spectral information can be recovered from data measured with as short on-off times as 1s.

The interpretation of inverted spectral IP models based on field data can be challenging since microgeometrical and microchemical factors are often unknown. However, the interpretation can be enhanced by knowledge of relationships obtained in lab studies. In addition, conceptual models of the pore scale geometry and chemical composition can aid interpretation of field data.

A general conclusion of this work is that much knowledge about granular silicate soils and sedimentary rocks have already been obtained in previous research (chapter 5). The established relationships should be possible to use qualitatively in field scale interpretation of spectral IP parameters, more or less, directly. For example, higher IP magnitude and shorter relaxation times could indicate more consolidated conditions in an otherwise homogeneous sandstone. Similarly, lower IP magnitude could indicate higher water content or saline groundwater. However, the interpretation of field scale data always requires knowledge of site-specific factors and a critical review of different possible sources to the observed signals.

The conclusions that can be drawn from the work on NAPL contaminated soil (presented in Johansson et al. 2015) is that it is difficult to correlate NAPL concentrations to IP variations in a similar way as groundwater salinity can be correlated to resistivity variations. The IP responses of NAPL contaminated soils are probably not only related to the contaminant concentrations, but also to other factors. One important factor that depends on the physical properties of the contaminants is the NAPLs influence on the pore geometry and the interfaces between different phases in the soil. The conceptual model of physical mechanisms in the pore space enhanced the interpretation of the field data in Johansson et al. (2015).

From the analysis of spectral IP responses of limestones (Johansson et al. 2016), the main conclusion is that similar IP responses can indicate different rock properties depending

on the mineral constituents of the rock. For example, geological weathering processes affect the physical properties of silicate and calcium carbonate rocks differently. The SEM and EDS-analysis gave an important insight into the microgeometry and mineralogical content of the investigated limestone. The microgeometry of the limestone is not well represented by many current IP mechanisms (chapter 5), which are based around the response of granular homogeneous soils and rocks. More research is needed to understand spectral IP behavior of limestones, for example, the possible effects of different fossil grain shapes and the degree of cementation.

9 References

Abdel Aal, G.Z., Slater, L.D. & Atekwana, E.A., 2006. Induced-polarization measurements on unconsolidated sediments from a site of active hydrocarbon biodegradation. *Geophysics*, 71(2), pp.H13–H24.

Atekwana, E.A. & Slater, L.D., 2009. Biogeophysics: A new frontier in Earth science research. *Reviews of Geophysics*, 47(4), pp.1–30.

Auken, E., Christiansen, A. V., Kirkegaard, C., Fiandaca, G., Schamper, C., Behroozmand, A. A., Binley, A., Nielsen, E., Effersø, F., Christensen, N.B., Sørensen, K., Foged, N. & Vignoli, G., 2014. An overview of a highly versatile forward and stable inverse algorithm for airborne, ground-based and borehole electromagnetic and electric data. *Exploration Geophysics*, 46(3), pp.223–235.

Bard, A.J. & Faulkner, L.R., 2001. *Electrochemical Methods Fundamentals and Applications* Second ed., John Wiley & Sons, Inc.

Bertin, J. & Loeb, J., 1976. *Experimental and Theoretical Aspects of Induced Polarization*, Berlin Stuttgart: Gebrüder Borntraeger.

Binley, A., Slater, L. D., Fukes, M., & Cassiani, G., 2005. Relationship between spectral induced polarization and hydraulic properties of saturated and unsaturated sandstone. *Water Resources Research*, 41(12), W12417.

Boadu, F.K. & Owusu-Nimo, F., 2010. Influence of petrophysical and geotechnical engineering properties on the electrical response of unconsolidated earth materials. *Geophysics*, 75(3), pp.G21–G29.

Brandes, I. & Acworth, I., 2003. Intrinsic Negative Chargeability of Soft Clays. In *Procs. ASEG 16th Geophysical Conference and Exhibition, February 2003, Adelaide*.

Butler, K.D., 2005. *Near-surface Geophysics* Investigat. K. D. Butler, ed.13, Society of exploration geophysicists.

Börner, F., Gruhne, M. & Schön, J., 1993. Contamination indications derived from electrical properties in the low frequency range. *Geophysical Prospecting*, 41(1), pp.83–98.

Cardarelli, E. & Di Filippo, G., 2009. Electrical resistivity and induced polarization tomography in identifying the plume of chlorinated hydrocarbons in sedimentary formation: a case study in Rho (Milan - Italy). *Waste Management & Research*, 27(6), pp.595–602.

Cassiani, G., Kemna, A., Villa, A., & Zimmermann, E., 2009. Spectral induced polarization for the characterization of free-phase hydrocarbon contamination of sediments with low clay content. *Near Surface Geophysics*, 7(5-6), pp.547–562.

Chambers, J. E., Loke, M. H., Ogilvy, R. D., & Meldrum, P. I., 2004. Non-invasive monitoring of DNAPL migration through a saturated porous medium using electrical impedance tomography. *Journal of contaminant hydrology*, 68, pp.1–22.

Cole, K.S. & Cole, R.H., 1941. Dispersion and Absorption in Dielectrics I. Alternating Current Characteristics. *The Journal of Chemical Physics*, 9, pp.341–351.

Dahlin, T. & Leroux, V., 2012. Improvement in time-domain induced polarization data quality with multi-electrode systems by separating current and potential cables. *Near Surface Geophysics*, 10, pp.545–565.

Dahlin, T., Leroux, V. & Rosqvist, H., 2010. Resistivity-IP mapping for landfill applications. *First Break*, 28(August), pp.101–105.

Dahlin, T. & Loke, M.H., 2015. Negative apparent chargeability in time-domain induced polarisation data. *Journal of Applied Geophysics*, 123, pp.322–332.

Dahlin, T. & Zhou, B., 2004. A numerical comparison of 2D resistivity imaging with 10 electrode arrays. *Geophysical Prospecting*, 52(5), pp.379–398.

Deceuster, J. & Kaufmann, O., 2012. Improving the delineation of hydrocarbon-impacted soils and water through induced polarization (IP) tomographies: a field study at an industrial waste land. *Journal of contaminant hydrology*, 136-137(August 2012), pp.25–42.

Dias, C.A., 2000. Developments in a model to describe low-frequency electrical polarization of rocks. *Geophysics*, 65(2), pp.437–451.

Fiandaca, G., Ramm, J., Binley, A., Gazoty, A., Christiansen, a. V., & Auken, E., 2013. Resolving spectral information from time domain induced polarization data through 2-D inversion. *Geophysical Journal International*, 192(2), pp.631–646.

Fiandaca, G., Auken, E., Christiansen, A. V., & Gazoty, A., 2012. Time-domain-induced polarization: Full-decay forward modeling and 1D laterally constrained inversion of Cole-Cole parameters. *Geophysics*, 77(3), pp.E213–E225.

Flores Orozco, A., Kemna, A., Oberdörster, C., Zschornack, L., Leven, C., Dietrich, P., & Weiss, H., 2012. Delineation of subsurface hydrocarbon contamination at a former hydrogenation plant using spectral induced polarization imaging. *Journal of contaminant hydrology*, 136-137, pp.131–44.

Flores Orozco, A., Williams, K. H., Long, P. E., Hubbard, S. S., & Kemna, A., 2011. Using complex resistivity imaging to infer biogeochemical processes associated with bioremediation of an uranium-contaminated aquifer. *Journal of Geophysical Research: Biogeosciences*, 116(3), pp.1–17.

Gazoty, A., Fiandaca, G., Pedersen, J., Auken, E., & Christiansen, A. V., 2012. Mapping of landfills using time-domain spectral induced polarization data: the Eskelund case study. *Near Surface Geophysics*, pp.575–586.

Iliceto, V., Santarato, G. & Veronese, S., 1982. An approach to the identification of fine sediments by induced polarization laboratory measurements. *Geophysical Prospecting*, 30, pp.331–347.

Iwamoto, M., 2012. Maxwell–Wagner Effect. In B. Bhushan, ed. *Encyclopedia of Nanotechnology*. pp. 1276–1285.

Johansson, S., Sparrenbom, C., Fiandaca, G., Lindskog, A., Olsson, P.-I., Dahlin, T., & Rosqvist, H., 2016. Investigations of a Cretaceous limestone with spectral induced polarization and scanning electron microscopy. *Submitted for publication (Geophysical Journal International)*.

Johansson, S., Fiandaca, G. & Dahlin, T., 2015. Influence of non-aqueous phase liquid configuration on induced polarization parameters: Conceptual models applied to a time-domain field case study. *Journal of Applied Geophysics*, 123, pp.295–309.

Jougnot, D., Ghorbani, A., Revil, A., Leroy, P., & Cosenza, P., 2010. Spectral induced polarization of partially saturated clay-rocks: a mechanistic approach. *Geophysical Journal International*, 180(1), pp.210–224.

Kemna, A., Binley, A., Cassiani, G., Niederleithinger, E., Revil, A., Slater, L., Williams, K.H., Flores Orozco, A., Haegel, F.-H., Hördt, A., Kruschwitz, S., Leroux, V., Titov, K &Zimmermann, E., 2012. An overview of the spectral induced polarization method for near-surface applications. *Near Surface Geophysics*, 10, pp.453–468.

Kemna, A., 2000. *Tomographic Inversion of Complex Resistivity - Theory and Application*. Ruhr-Universität Bochum.

Koch, K., Kemna, A., Irving, J., & Holliger, K., 2011. Impact of changes in grain size and pore space on the hydraulic conductivity and spectral induced polarization response of sand. *Hydrology and Earth System Sciences*, 15(6), pp.1785–1794.

Leroy, P., Revil, A, Kemna, A, Cosenza, P., & Ghorbani, A, 2008. Complex conductivity of water-saturated packs of glass beads. *Journal of colloid and interface science*, 321(1), pp.103–17. Available at: http://www.ncbi.nlm.nih.gov/pubmed/18272167 [Accessed May 29, 2013].

Leroy, P., & Revil, A., 2009. A mechanistic model for the spectral induced polarization of clay materials. *Journal of Geophysical Research: Solid Earth*, 114(B10202).

Lesmes, D. & Friedman, S., 2005. Hydrogeophysics. In Y. Rubin and S. S. Hubbard, ed. Springer, pp. 87–128.

Lesmes, D.P. & Frye, K.M., 2001. Influence of pore fluid chemistry on the complex conductivity and induced polarization responses of Berea sandstone. *Journal of Geophysical Research*, 106(B3), pp.4079–4090.

Lesmes, D.P. & Morgan, F.D., 2001. Dielectric spectroscopy of sedimentary rocks. *Journal of Geophysical Research*, 106(B7), pp.13329–13346.

de Lima, O.A.L. & Sharma, M.M., 1992. A generalized Maxwell-Wagner theory for membrane polarization in shaly sands. *Geophysics*, 57(3), pp.431–440.

Magnusson, M.K., Fernlund, J.M.R. & Dahlin, T., 2010. Geoelectrical imaging in the interpretation of geological conditions affecting quarry operations. *Bulletin of Engineering Geology and the Environment*, 69(3), pp.465–486.

Marshall, D.J. & Madden, T.R., 1959. Induced polarization, a study of its causes. *Geophysics*, XXIV(4), pp.790–816.

Martinho, E., Almeida, F. & Senos Matias, M.J., 2006. An experimental study of organic pollutant effects on time domain induced polarization measurements. *Journal of Applied Geophysics*, 60(1), pp.27–40.

Nordsiek, S. & Weller, A., 2008. A new approach to fitting induced-polarization spectra. *Geophysics*, 73(6), pp.F235–F245.

Ntarlagiannis, D. et al., 2005. Low-frequency electrical response to microbial induced sulfide precipitation. *Journal of Geophysical Research*, 110(G2).

Olhoeft, G.R., 1985. Low frequency electrical properties. *Geophysics*, 50(12), pp.2492–2503.

Olsson, P.-I., Fiandaca, G., Larsen, J. J., Dahlin, T., & Auken, E., 2016. Doubling the spectrum of time-domain induced polarization: removal of non-linear self-potential drift, harmonic noise and spikes, tapered gating, and uncertainty estimation. *Submitted for publication (Geophysical Journal International)*.

Pelton, W. H., Ward, S. H., Hallof, P. G., Sill, W. R., & Nelson, P. H., 1978. Mineral discrimination and removal of inductive coupling with multifrequency IP. *Geophysics*, 43(3), pp.588–609.

Personna, Y. R., Slater, L., Ntarlagiannis, D., Werkema, D., & Szabo, Z., 2013. Complex resistivity signatures of ethanol in sand-clay mixtures. *Journal of contaminant hydrology*, 149(2013), pp.76–87.

Powers, M.H., 1997. Modeling frequency-dependent GPR. *The Leading Edge*, 16(11), pp.1657–1662.

Revil, A., 2012. Spectral induced polarization of shaly sands: Influence of the electrical double layer. *Water Resources Research*, 48(2).

Revil, A. & Florsch, N., 2010. Determination of permeability from spectral induced polarization

in granular media. *Geophysical Journal International*, 181(3), pp.1480–1498.

Revil, A., Koch, K. & Holliger, K., 2012. Is it the grain size or the characteristic pore size that controls the induced polarization relaxation time of clean sands and sandstones? *Water Resources Research*, 48(5).

Schmutz, M., Revil, A., Vaudelet, P., Batzle, M., Viñao, P. F., & Werkema, D. D., 2010. Influence of oil saturation upon spectral induced polarization of oil-bearing sands. *Geophysical Journal International*, 183(1), pp.211–224.

Scott, J.B.T. & Barker, R.D., 2003. Determining pore-throat size in Permo-Triassic sandstones from low-frequency electrical spectroscopy. *Geophysical Research Letters*, 30(9).

Seigel, H.O., 1959. Mathematical formulation and type curves for induced polarization. *Geophysics*, XXIV(3), pp.547–565.

Sen, P.N., 1981. Relation of certain geometrical features to the dielectric anomaly of rocks. *Geophysics*, 46(12), pp.1714–1720.

Sen, P.N., Scala, C. & Cohen, M.H., 1981. A self-similar model for sedimentary rocks with application to the dielectric constant of fused glass beads. *Geophysics*, 46(5), pp.781–795.

Slater, L. & Lesmes, D.P., 2002a. Electrical-hydraulic relationships observed for unconsolidated sediments. *Water Resources Research*, 38(10), pp.1–13.

Slater, L.D. & Lesmes, D., 2002b. IP interpretation in environmental investigations. *Geophysics*, 67(1), pp.77–88.

Sumner, J.S., 1976. *Principles of induced polarization for geophysical exploration*, Amsterdam: Elsevier Scientific Publishing Company.

Titov, K., Kemna, A., Tarasov, A., & Vereecken, H., 2004. Induced Polarization of Unsaturated Sands Determined through Time Domain Measurements. *Vadose Zone Journal*, 3(4), pp.1160–1168.

Titov, K., Komarov, V., Tarasov, V., & Levitski, A., 2002. Theoretical and experimental study of time domain-induced polarization in water-saturated sands. *Journal of Applied Geophysics*, 50(4), pp.417–433.

Ustra, A., Slater, L., Ntarlagiannis, D., & Elis, V., 2012. Spectral Induced Polarization (SIP) signatures of clayey soils containing toluene. *Near Surface Geophysics*, 10, pp.503–515.

Vanhala, H., 1997. Mapping oil-contaminated sand and till with the spectral induced polarization (SIP) method. *Geophysical Prospecting*, 45(2), pp.303–326.

Ward, S., 1988. The resistivity and induced polarization methods. In *1st EEGS Symposium on the Application of Geophysics*.

Weller, A. & Slater, L.D., 2015. Induced polarization dependence on pore space geometry : Empirical observations and mechanistic predictions. *Journal of Applied Geophysics*, 123, pp.310–315.

Vinegar, H.J. & Waxman, M.H., 1984. Induced polarization of shaly sands. *Geophysics*, 49(8), pp.1267–1287.

Wong, J., 1979. An electrochemical model of the induced-polarization phenomenon in disseminated sulfide ores. *Geophysics*, 44(7), pp.1245–1265.

Van Voorhis, G.D., Nelson, P.H. & Drake, T.L., 1973. Complex resistivity spectra of porphyry copper mineralization. *Geophysics*, 38(1), pp.49–60.

Zhang, C., Slater, L., Redden, G., Fujita, Y., Johnson, T., & Fox, D., 2012. Spectral induced polarization signatures of hydroxide adsorption and mineral precipitation in porous media. *Environmental Science and Technology*, 46(8), pp.4357–4364.

Zisser, N., Kemna, A. & Nover, G., 2010. Relationship between low-frequency electrical

properties and hydraulic permeability of low-permeability sandstonesRelationship. *Geophysics*, 75(3), pp.E131–E141.

Zonge, K.L., Sauck, W.A. & Sumner, J.S., 1972. Comparison of time, frequency and phase measurements in induced polarization. *Geophysical Prospecting*, 20(3), pp.626–648.

BeFo

Box 5501
SE-114 85 Stockholm

info@befoonline.org • www.befoonline.org
Visiting address: Storgatan 19, Stockholm

ISSN 1104-1773